AD-A119 309 JOHNS HOPKINS UNIV LAUREL MD APPLIED PHYSICS LAB F/G 17/7
FIXED SITE COMPARISON OF P AND C/A CODE RANGING PERFORMANCE USI--ETC(U)
APR 82 G D BAILEY
UNCLASSIFIED APL/JHU-S2T-82-038 USCG-D-30-82 NL

END
DATE FILMED
10-82
DTIC

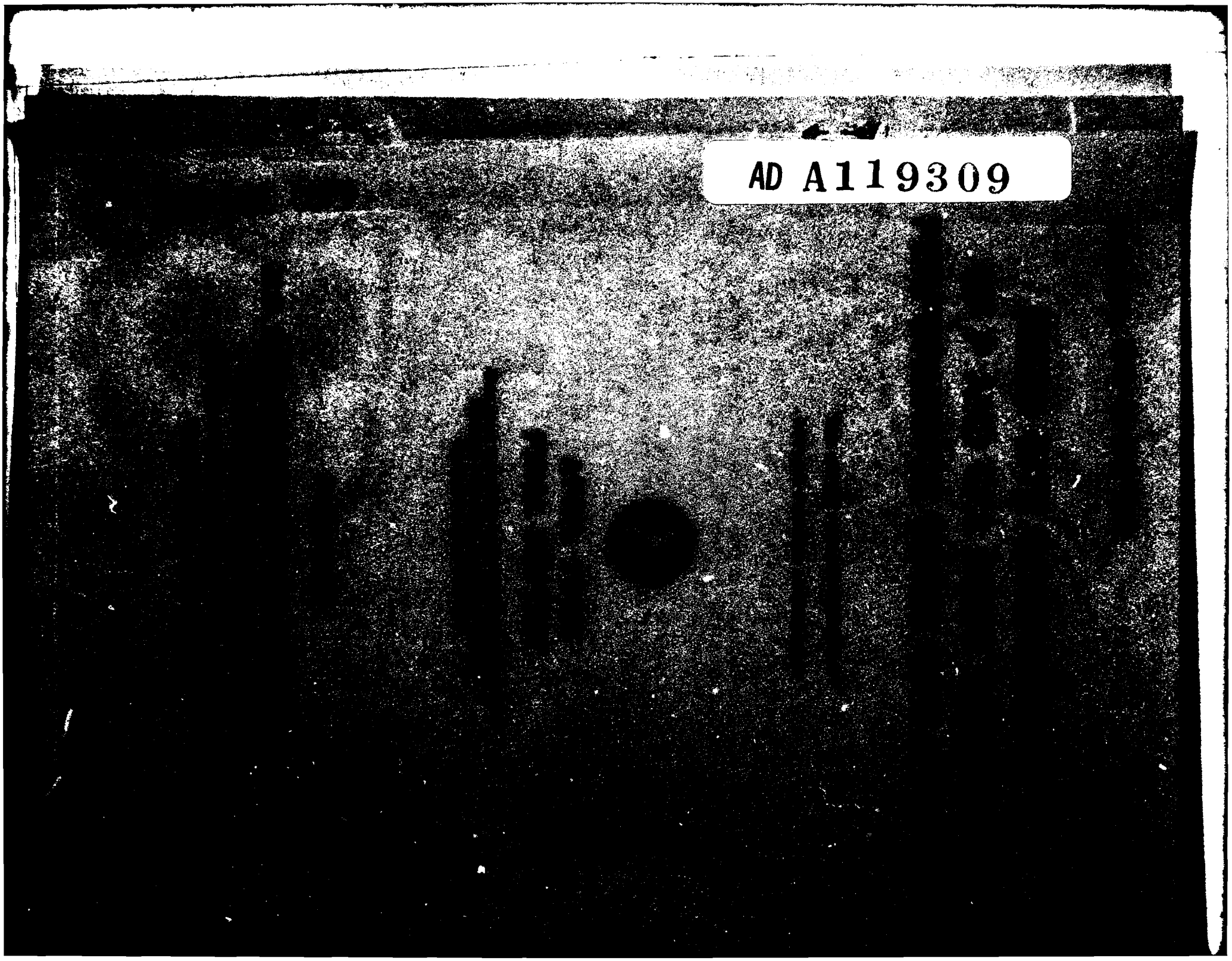

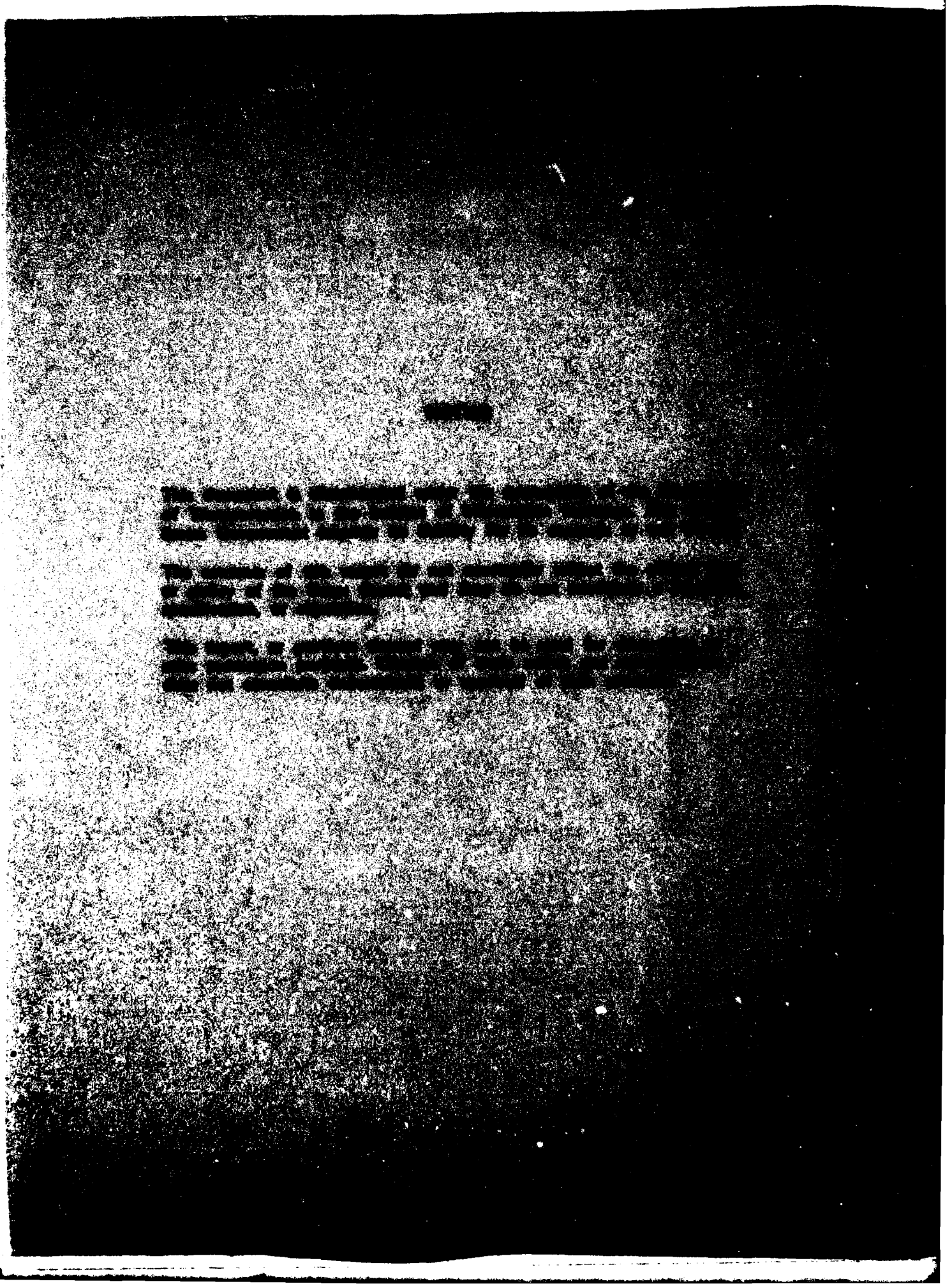

METRIC CONVERSION FACTORS

Approximate Conversions to Metric Measures

Symbol	When You Know	Multiply by	To Find	Symbol
	LENGTH			
	inches	*2.5	centimeters	
	feet	30	centimeters	
	yards	0.9	meters	
	miles	1.6	kilometers	
	AREA			
	square inches	6.5	square centimeters	
	square feet	0.09	square meters	
	square yards	0.8	square meters	
	square miles	2.6	square kilometers	
	acres	0.4	hectares	
	MASS (weight)			
	ounces	28	grams	
	pounds	0.45	kilograms	
	short tons (2000 lb)	0.9	tonnes	
	VOLUME			
	teaspoons	5	milliliters	
	tablespoons	15	milliliters	
	fluid ounces	30	milliliters	
	cups	0.24	liters	
	pints	0.47	liters	
	quarts	0.95	liters	
	gallons	3.8	liters	
	cubic feet	0.03	cubic meters	
	cubic yards	0.76	cubic meters	
	TEMPERATURE (exact)			
°F	Fahrenheit temperature	5/9 (after subtracting 32)	Celsius temperature	°C

*1 in = 2.54 (exactly). For other exact conversions and more detailed tables, see NBS Misc. Publ. 286, Units of Weights and Measures. Price $2.25, SD Catalog No. C13.10:286.

Approximate Conversions from Metric Measures

Symbol	When You Know	Multiply by	To Find	Symbol
	LENGTH			
	millimeters	0.04	inches	
	centimeters	0.4	inches	
	meters	3.3	feet	
	meters	1.1	yards	
	kilometers	0.6	miles	
	AREA			
	square centimeters	0.16	square inches	
	square meters	1.2	square yards	
	square kilometers	0.4	square miles	
	hectares (10,000 m²)	2.5	acres	
	MASS (weight)			
	grams	0.035	ounces	
	kilograms	2.2	pounds	
	tonnes (1000 kg)	1.1	short tons	
	VOLUME			
	milliliters	0.03	fluid ounces	
	liters	2.1	pints	
	liters	1.06	quarts	
	liters	0.26	gallons	
	cubic meters	35	cubic feet	
	cubic meters	1.3	cubic yards	
	TEMPERATURE (exact)			
°C	Celsius temperature	9/5 (then add 32)	Fahrenheit temperature	°F

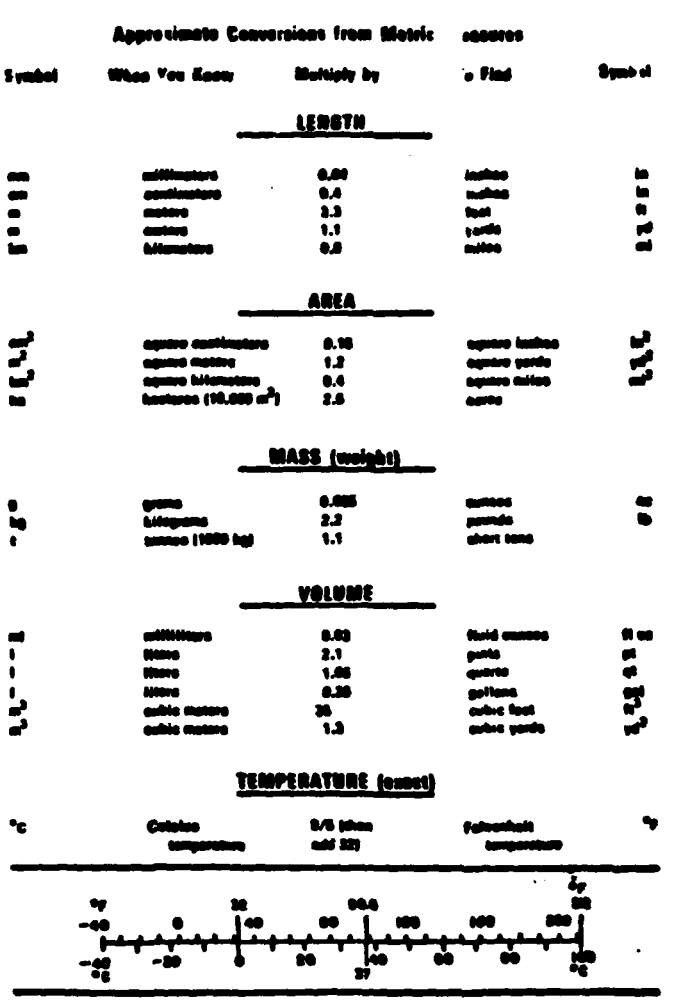

Technical Report Documentation Page

1. Report No.	2. Government Accession No.	3. Recipient's Catalog No.
CG-D-30-82	AD-A119 305	

4. Title and Subtitle
Fixed Site Comparison of P and C/A Code Ranging Performance Using GPS X-Sets

5. Report Date
April 1982

6. Performing Organization Code

7. Author(s)
Gregory D. Bailey

8. Performing Organization Report No.
S2T-82-038

9. Performing Organization Name and Address
The Johns Hopkins University
Applied Physics Laboratory
Johns Hopkins Road
Laurel, Maryland 20810

10. Work Unit No. (TRAIS)
2262

11. Contract or Grant No.

12. Sponsoring Agency Name and Address
Department of Transportation
U. S. Coast Guard
Office of Research and Development
Washington, DC 20593

13. Type of Report and Period Covered
Final Report
July 1981 to December 1981

14. Sponsoring Agency Code
G-DST-1

15. Supplementary Notes

16. Abstract

The NAVSTAR Global Positioning System (GPS) is a satellite-based navigation system under development by the Department of Defense. Satellites transmit a precise (P) code and a clear/acquisition (C/A) code which are used to calculate satellite to user range. Ranges from three or more satellites are then used to determine the user's position. The Johns Hopkins University Applied Physics Laboratory (APL) has two identical receivers, each of which is capaple of tracking either code. The purpose of the study was to examine the characteristics of the C/A code as it might be used by a marine user with a low-cost GPS receiver. Thirty-three days of data were taken between 7/29/81 and 12/16/81. The study found that the single-frequency P and C/A code range residuals and navigation errors show the same basic characteristics, except for expected higher noise levels in the C/A code, and possible multi-path interference in the C/A code of one satellite as it set. The dual-frequency P code phase delay measurements provided ionospheric corrections that appeared reasonable in character and value. The ionospheric contribution to position error was found to be largest when two of four satellites were at low elevation. At other times the ionospheric effect on position error appeared negligible.

17. Key Words	18. Distribution Statement
NAVSTAR GPS, Satellite navigation, Satellite ranging, Multipath interference	This document is available to the U. S. public through the National Technical Information Service, Springfield, VA 22161

19. Security Classif. (of this report)	20. Security Classif. (of this page)	21. No. of Pages	22. Price
Unclassified	Unclassified		

Form DOT F 1700.7 (8-72) Reproduction of completed page authorized

ACKNOWLEDGMENTS

The author wishes to acknowledge the following APL staff members for their valuable assistance rendered during the course of this study: E. F. Prozeller, R. J. Heins, W. C. Trimble, D. J. Duven, R. R. Yost, Jr., W. E. Tye, and M. M. Feen.

Gregory D. Bailey

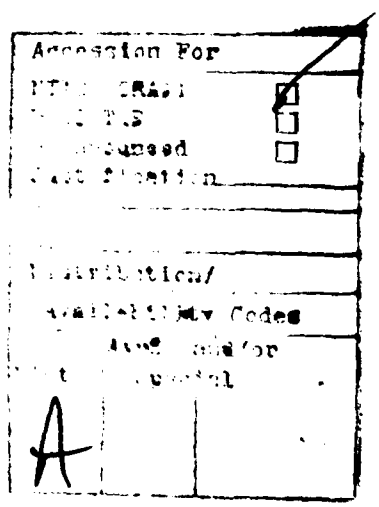

PREFACE-

a. The SATRACK Ionospheric Monitor Station facility at APL/JHU contains two identical X-sets, each of which is capable of tracking the GPS P or C/A ranging codes. The objective of the study was to examine the characteristics of single-frequency L1 C/A-code navigation such as a marine user with a low-cost GPS navigation set might experience. One X-set was assigned to track L1 P-codes and the other to track L1 C/A codes, simultaneously from the same four satellites, providing a unique opportunity to compare the ranging performance of the two codes based on fixed site operations at APL.

b. In support of the USCG study, 33 days of data were recorded between 7/29/81 and 12/16/81. The goal of recording extensively with the side-by-side X-sets was thwarted by a faulty power supply on X-set 2 on 9/15/81. Throughout the remainder of the data gathering period, the remaining X-set was assigned to track the P codes and the C/A codes on alternate days. Appendix B contains a tape log and processing summary.

c. In the study it was found that single-frequency P and C/A-code pseudorange residuals and navigation error results exhibit the same basic characteristics, with the exception of the inherently higher noise level on the C/A-code data and possible C/A-code multipath interference on an easterly setting satellite (NAVSTAR 4). The dual-frequency P-code phase delay measurements available from the X-set were found to provide consistent ionospheric measurements that appear reasonable in character and value. The ionospheric contribution to position error was found to be prominent at times when two of the four satellites were at low elevation angles - early or late in the pass. At other times the contribution appeared to be similar enough on all four signals that it did not substantially affect the horizontal position error.

CONTENTS

1. BACKGROUND.

a. Global Positioning System (GPS)

(1) The Global Positioning System (GPS) consists presently of a constellation of 6 satellites in 2-orbit planes, each inclined 63° with respect to the equatorial plane and offset from each other by 120° in longitude. The orbit period of 11 h 57m 58.3 s (one-half sidereal day) was selected to produce a fixed ground track for each satellite, causing the earth-fixed subsatellite point to return to a given point in its ground track about 4 minutes earlier each day.

(2) Of the six satellites in orbit four have clocks suitable for accurate navigation. Each satellite transmits two signals referred to as the L1 signal with center frequency of 1575.42 MHz and the L2 signal with center frequency of 1227.6 MHz. The dual frequency signal structure allows measurement, at the receiver, of ionospheric time delay error.

(3) GPS is a ranging system whereby range is inferred from ranging code epoch receipt time measurements. Both L1 and L2 signals are modulated by a 10.23 MHz clock rate precision (P) ranging code, used for precise navigation, which offers substantial jamming immunity and repeats itself once every 7 days.

(4) The L1 signal, in addition, is modulated by a 1.023 MHz clock rate clear/acquisition (C/A) ranging code, which offers ease of acquisition due to its one-millisecond period. Acquisition of the C/A code and recovery of a single full subframe of the satellite navigation message data permit the P code to be acquired with little or no search.

(5) The navigation message transmitted by each satellite is a 50-bit per second data stream common to both the P and C/A signals. It contains precise satellite ephemerides, system time, satellite clock behavior data, transmitter status information and C/A-to-P signal handover information. Each satellite also transmits almanacs containing coarse ephemerides and clock offsets for all satellites in the constellation. The high precision ephemeris allows the user to calculate satellite position at the time of transmission of the signal, one step in determining the range.

(6) The highly stable atomic frequency standard clocks in the satellites have predictable offsets and drift rates with respect to GPS system time, which is maintained by the Master Control Station (MCS) by means of a set of cesium clocks. The MCS monitors the individual satellite clocks daily and generates clock correction parameters which are transmitted to the satellites where they are then retransmitted, along with the ephemeris and almanac data, in the navigation message. These parameters allow the user to determine the precise magnitudes of satellite clock offsets. The MCS is capable of adjusting the phase and frequency of each satellite clock to maintain the clock operation within limits.

(7) A user can measure the time of arrival of the signal and infer a pseudorange from the measured transit time. Even with precise knowledge of the transmit time (relative to GPS system time) his measurement of the transit time

will be in error by the offset between his receiver clock and GPS time. A user with an unknown position and clock offset can solve for his position in three dimensions and his clock offset by using simultaneous pseudorange measurements from a minimum of four satellites. A user with a clock synchronized to GPS system time needing to solve only for his position in three dimensions needs measurements from only three satellites. Likewise, a user who knows his altitude (such as sea level) needing to solve only for his clock offset and position in the tangent plane also requires only three satellites.

(8) The X-set receiver clock was driven in these experiments by a frequency standard at APL with a known drift rate relative to Coordinated Universal Time (UTC) as maintained by the U.S. Naval Observatory (USNO). The difference between UTC and GPS time is measured daily at the USNO by tracking the satellites with a GPS timing receiver. This difference has two components: (1) a difference due to drift between UTC and GPS time, and (2) a difference of an integer number of seconds because UTC introduces discrete leap seconds into its timekeeping periodically, while GPS, because of the requirement for constant availability for navigation, does not. In these experiments, the measured UTC-GPS difference values determined from NAVSTARS 3, 4, 5, and 6 were generally within 0.1 μ sec of each other and were in the range 50-60 μ sec after accounting for the 3 leap seconds. This approximate 3-second clock difference would appear as an error in pseudorange (transit time) common to all satellites and would not affect user position error in a navigation solution which included solving for the user clock error.

(9) In our experiments the measured pseudorange data were not used to navigate a user position and clock offset as a marine user would using an algorithm within the X-set. Instead, because the antenna position is known precisely, the satellite ephemeris data were used to calculate the theoretical slant range to the satellite, and the difference between the measured pseudorange and theoretical range was computed as the pseudorange error or residual.

(10) The magnitude of the user position or navigation error is determined by the combination of the ranging errors and the geometry of the user and the satellites being tracked. A measure of the geometric effects is contained in geometric dilution of precision (GDOP) terms, large values indicating a poor navigation solution due to unfavorable satellite geometry and causing a magnification of the ranging error. One of these GDOP parameters, HDOP is of primary concern to a marine user assumed to have knowledge of his altitude. HDOP is the dilution of precision in the horizontal plane and is defined mathematically as:

$$HDOP = \sqrt{\sigma_{xx}^2 + \sigma_{yy}^2}$$

here σ_{xx} and σ_{yy} are the variances of the estimated user position in the X and Y axes due to geometry only (Ref. 1). Appendix C contains a more detailed discussion of HDOP.

(11) The volume containing Ref. 1 is a collection of papers dealing with many aspects of the Global Positioning System and is a good source of background material.

b. The APL GPS Monitor Station: The GPS Monitor station at APL consists of two X-sets, a display station, and a tape recorder as shown in Fig. 1.

(1) X-Sets. Each X-set consists of a receiver capable of simultaneous reception of four satellite signals on independent channels, a data processor, and a control/display unit.

(a) X-Receiver:

(1) A functional diagram of the receiver portion of the X-set is shown in Fig. 2. Its major components are four carrier channels, a code channel, and a process controller.

(2) Each carrier channel performs detection, carrier tracking, and data demodulation on the L1 or L2 signal from a single satellite, and contains a hardware PRN code generator which produces a local code signal to be correlated with the received signal. Each code generator is capable of generating all the unique PRN code sequences for both the P and C/A codes from all the satellites.

(3) The code channel receives PRN code sequences generated by each of the four carrier channels, and performs cross-correlation between the code channel input signal and each locally generated code sequence, one sequence at a time. When an L1 P code is being tracked in a carrier channel, the associated L2 signal is assigned to the code channel, and an adjustable delay in the code channel is incremented to match the L2 P code being received. The amount of delay required to obtain peak correlation is a direct measurement of the difference in arrival times of the L1 and L2 signals.

(4) The process controller is responsible for real time control of the X-receiver operation. It controls the acquisition and tracking of carriers and codes, the measurement circuitry, and the hardware clock. It also monitors receiver health and status.

(b) Data Processor:

(1) The data processor, an HP 2108 computer, controls receiver initialization allowing the user to select carriers and codes; receives the health, status, and measurement data for processing; and maintains the software which performs the navigation solution.

(2) The output of the data processor consists of User Field Test Instrumentation (UFTIN) data blocks. A number of data block types, providing information about the operation of the X-set, are available from the processor. The primary blocks of interest in this study contain the pseudorange measurement data (block 6), the received satellite ephemeris data (blocks 20, 21, 22, 23), and the ionospheric measurement data (block 8).

(c) Control Display Unit: The Control Display Unit (CDU) is a CRT terminal connected to the data processor through which a user can control receiver initialization, set the X-set hardware clock, enter program modifications, and display certain receiver parameters.

(2) Display Station and Tape Recorder:

(a) The display station consists of an APL-designed data controller, an HP 2641 CRT terminal, an HP 2108 computer with disk driver, and a Kennedy 9000-1/9232 9-track tape recorder.

(b) The UFTIN data blocks created by the X-set data processor are routed directly to the data controller. The controller time multiplexes the data from the two X-sets and allows the operator to switch-select particular data blocks for display and/or recording.

(c) The display station computer contains two programs which are used for data display and control of the tape recorder. The display program formats and displays on the screen certain health, status, and measurement words which indicate what is happening with each channel in an X-set. Figure 3 shows the information in a screen display during tracking as derived from UFTIN block 6 data. Each channel is assigned to track the same signal; the data are dispayed in octal format for each channel of the receiver. Detailed descriptions of the displayed words are contained in Ref. 2. The tape recorder program formats all data blocks passed by the data controller and passes them to the tape recorder for processing at a later time via the APL computing facilities.

(3) Operation of the APL X-set Station: Operation of the APL X-set station requires a number of general steps, summarized as follows: loading the software and a recent almanac into the data processor, setting the hardware clock within the X-receiver, initialization of the receiver, selection of satellite assignments and data rate, and loading and running of the display and recorder programs.

(a) Load Software and Recent Almanac Into Data Processor: The software delivered with the X-set (Ref. 2) performs very specific functions; however, it can be made more flexible by entering program modifcations (developed by APL) via the X-set control display unit. The original program, for example, automatically directs all four receiver channels to the same carrier frequency and code, and makes the satellite assignments based on its own calculations of GDOPs.

(1) A number of modifications were made to the basic software program to make better use of the versatility of the hardware. The X-set clock can now be set to within a few microseconds of UTC instead of to one of the satellite clocks. The automatic search and acquisition programs remain intact, but the software no longer attempts to solve for user position. The program modifications allow the operator to independently select the key parameters for each receiver channel, namely: code (P or C/A), frequency (L1 or L2), and satellite (0 through 32).

(2) The receiver must know roughly where a satellite is before it can acquire the signal because of the large variation possible in the Dopper effect on the signal. An almanac is transmitted by all satellites and contains ephemeris data of quality sufficient to allow the receiver to tune for acquisition of any satellite. To acquire a particular satellite the almanac must be obtained from another satellite or from the same satellite at an earlier time. The almanac is updated internally by a tracking X-set as the satellites transmit a periodically updated message. A current almanac can be loaded by itself or as part of the total memory from the receiver onto a cassette tape for storage. Likewise, a recent almanac or the entire contents of memory can be loaded back into the X-set from the cassette.

(b) Setting of Hardware Clock Within X-Receiver: The hardware clock within the receiver is driven by a 5 MHz reference oscillator in the APL Time and Frequency Laboratory (TFL). In early experiments this oscillator was a cesium standard with a regularly measured drift rate with respect to UTC. In later experiments the 5 MHz was derived from a hydrogen maser. The X-set hardware clock normally runs constantly, but in the event of a power failure or a problem with the oscillator the clock must be reset. The setting of the clock can be accomplished in two ways:

(1) The receiver can be directed via the data processor terminal to set its clock to the clock in the first satellite acquired and tracked. To a user without knowledge of his initial clock error, such as an isolated marine user, this would be the normal mode of operating.

(2) The clock can be set via the terminal to a user selected time at the incidence of a synchronization pulse from the TFL. This pulse is maintained within microseconds of UTC by adjusting its phase to offset the drift between UTC and the cesium standard in the TFL. This is the normal mode of operation for the experiments described in this report.

(c) Initialization of Receiver. The receiver must have certain parameter values set prior to tracking. The frequency and code to be tracked and user position must be entered via the terminal. In these experiments each X-set was assigned to track only the L1 C/A code or the L1 P code from all four satellites.

(d) Selection of Satellite Assignments and Data Rate. The user can direct each channel's satellite assignment and the overall receiver data rate by setting values in key memory locations via the terminal. The process controller designates to each receiver channel which satellite to acquire and an estimate of the expected Doppler shift on the signal. When the appropriate code sequences are synchronized, tracking of both the code sequence timing and carrier phase takes place.

(e) Loading and Running of Display and Recorder Programs. The program to display certain data words and to control the tape recorder reside on disc and must be loaded into the display station computer. The display program presents on the terminal certain status and measurement words for each carrier channel of the receiver. The tape recorder program is started when the satellites are acquired and the data are written on a 9-track magnetic tape via the Kennedy tape recorder.

2. GPS EXPERIMENTS AT APL.

(a) Objective of Study: A low cost GPS navigation set is of great interest to marine users. Such a set would likely be based on single frequency L1 C/A-code tracking. The objective of this study is to examine the characteristics of this simpler mode of navigation. Full dual frequency P-code navigation represents the best case available in which the user has all available code precision and can correct the data for measured ionospheric effects. By comparing L1 C/A-code navigation with the optimal dual frequency P-code navigation we hope to find what sacrifices are to be expected by a single frequency user. Expected problem areas are: ionospheric refraction effects on L1 and potential C/A-code measurement error sources not present with the P-code signal (e.g., multipath). Having two X-sets side-by-side allows the unique opportunity to compare these two modes of navigation by simultaneously tracking the L1 C/A code on one X-set and the dual frequency P code on the other.

(b) Experimental Methodology:

(1) The experiments in this study were all based on simultaneous tracking of four GPS satellites, NAVSTARs 3, 4, 5, and 6, whose orbits had been chosen to produce fixed ground tracks, providing a pass geometry that is regular from day to day. Figure 4 is a sterographic projection, centered at APL, of the satellite ground tracks for a 4-hour period beginning at 2300 GMT on day 81.233 (year 1981, day 233). The position of the satellites at hourly intervals past 2300 GMT are marked on the tracks. The outermost ring represents 0° elevation angle; the others are spaced at 20° intervals. These four satellites are visible at APL for a 3-1/2 hour daily pass interval; however, the satellites follow these fixed tracks about 4 minutes earlier each day.

(2) System timing, which is fundamental to ranging measurements, is diagrammed in Figure 5. GPS system time is maintained by the Master Control Station (MCS) at Vandenberg AFB, California. To provide continuous navigation capability, GPS time is continuous and no leap seconds are inserted. The MCS

tracks all satellites in the constellation and determines the differences between each of the satellite clocks and GPS time. The clock error, ΔT_{SV}, for each satellite is modeled as a second order polynomial in time and uploaded to the appropriate satellite for inclusion in the transmitted satellite message. In tracking a satellite each X-set records, as part of the satellite message, the clock error polynomial by which the user corrects the measured transit time of the signal. The accuracy of using these transmitted clock correction terms deteriorates as the age of the terms increases; the nominal period of applicability of these terms has been chosen to be one hour with one-half hour additional applicability after the data have changed (Ref. 3).

(3) Coordinated Universal Time (UTC) is maintained by the USNO. Periodic leap seconds are inserted in UTC, resulting in a current gross offset of 3 leap seconds between UTC and GPS. The USNO daily measures the difference between UTC and GPS system time by tracking each of the satellites with a GPS timing receiver and makes these data available from an observatory data bank.

(4) The clock in the X-set was driven early in this set of experiments by a cesium clock and later by a hydrogen maser clock, both of which are maintained by the Time and Frequency Laboratory (TFL) at APL. The maser and cesium clocks are independent of both UTC and GPS time; however, the TFL makes routine weekly measurements to determine the relative offset and drift rate between UTC and the TFL cesium clock. Neither the cesium nor maser clock at APL is corrected to maintain it close to UTC; however, a one pulse per second signal derived from the cesium clock is adjusted in phase to offset the measured TFL-UTC drift rate. This corrected signal is maintained within 1.5 μ sec of UTC and is used to set the X-set clock after introducing a delay to account for the current 3 leap seconds.

(5) Each X-set was assigned in this series of experiments to track only the L1 C/A codes or the L1 P codes in all four of its carrier channels. When L2 P codes were tracked in carrier channels, the X-set code channel was assigned to track the appropriate L2 P code for each satellite, so that the ionospheric effect could be determined from the L2-L1 differential delay. A data rate of 1 minute was chosen for each X-set, based on the cost and manageability of downstream processing of the data.

(6) At the conclusion of a pass, the magnetic tape containing the X-set data was processed in the McClure Computing Center using A P L language programs to perform the necessary calculations and generate the plots used to evaluate the data. Figure 6 is a functional illustration of the processing flow for the data from one X-set; when a tape contained data from both X-sets, the data were sorted and processed separately.

(7) The three types of data from each X-set used in these experiments are pseudorange measurements, ephemeris, and L2-L1 P-code differences. A pseudorange measurement point consists of a measurement time and one pseudorange measurement for each channel. The measurements were corrected,

during processing, for the satellite clock errors, using the appropriate polynomials. The clock corrected P-code pseudoranges were then corrected for ionospheric effects by calculating the correction at L1 for each satellite signal, at a time t_i, based on the L2-L1 P-code difference data and subtracting the corrections from the measured pseudoranges. This step was not included in the C/A-code processing since ionospheric range corrections are not available when L1 C/A-code signals are tracked, since the L2 signal is not modulated by the C/A code.

(8) The theoretical ranges to the four satellites at each pseudorange measurement time are calculated from orbit parameters contained in the ephemeris messages received from the satellites. The difference, at a time t_i, between the theoretical range to a satellite and the measured pseudorange, either corrected or uncorrected for ionosphere, is the ranging error or pseudorange residual. The four residuals were translated into navigation errors by means of a matrix calculation, based on the geometry of APL and the four satellites, as described in Appendix C.

3. EXPERIMENTAL RESULTS.

a. Tracking the Same Signals on Both X-sets: Before comparing the results of tracking the P code on one X-set and the C/A code on the other, both sets were assigned to track the same set of signals for the purpose of observing any inter-receiver differences in measured data. Channels 1, 2, 3, and 4 of each receiver were assigned to track the L1 P code from NAVSTARS 3, 4, 5, and 6, respectively, on day 81.233 (year 1981, day 233). The code channel of each receiver was assigned to track the L2 P codes so that an ionospheric measurement could be made on each satellite's signal. X-set-to-X-set comparison was made of pseudorange residuals, ionospheric range corrections, and navigation errors.

(1) Pseudorange Residuals:

(a) The pseudorange residuals produced by X-set 1 are shown in Fig. 7 and the corresponding residuals from X-set 2 are shown in Fig. 8. The horizontal axis is time in minutes past a reference time TØ, the hour, in Greenwhich Mean Time (GMT), preceding the first data point. Tick marks are shown at 10-minute intervals and accent marks are shown at 1-hour intervals past TØ. The vertical scale is measured minus theoretical pseudorange in microseconds and was selected automatically by the plotting software. Tick marks are shown at 9-meter (0.03 μ sec range equivalent) intervals. The statistical table on each plot shows, for each satellite, the average, the sigma about the average, the number of points, and the difference between the two most extreme values plotted.

(b) The data rate was 1 minute for each X-set, but because the receivers do not take data synchronously, no point-by-point comparison can be made between the two sets of data. The 25-minute gap in the X-set 2 data is due to loss of track in one or more of the receiver channels. During the approximately 3 hours of tracking, it can be seen that the gross shapes of the data as a function of time are the same.

(c) If all parameters in the system are known exactly, the pseudorange residuals for each satellite should have a zero average value and a flat curve over the duration of the pass. The data in Figs. 7 and 8, though, show average values in the range of -53 μsec to -54 μsec and have nonzero slopes. Most of the pseudorange bias seen on both X-sets is due to the offset between UTC and GPS time which was measured by the USNO for day 81.233 to be approximately -49 μsec. A smaller part of this common pseudorange bias is due to accumulated drift between UTC and the X-set clocks. The two X-set clocks both have the same drift rate relative to UTC or to GPS due to their common TFL oscillator source, so that if both clocks were set to UTC at the same time, their common drift would produce a common offset from UTC and from GPS time.

(d) A clock error in a receiver is the amount that the receiver time differs from GPS time. The time of receipt measurements will be in error and, thus, all pseudorange measurements made by the receiver will be too large or too small by the amount of the clock error. In a navigation solution which includes solving for the user clock error, though, the magnitude of this clock error does not affect the horizontal position error.

(e) If only one of the X-set clocks is reset to UTC, time as measured in each clock will be different. This difference will be due to the drift that has occurred in the TFL oscillator between the times that the two X-set clocks were set to UTC, and will be a source of pseudorange bias between receivers. If the two receivers track the same set of signals, with all conditions equal except for different receiver clock errors, the position errors resulting from their measured pseudoranges will not reflect the difference in clock errors.

(f) The residual data from both X-sets also show (Figs. 7 and 8) a common monotonic decrease in value with time over the entire pass for NAVSTARS 5 and 6, and out to approximately 120 minutes past T0 for NAVSTARS 3 and 4, at which time they are reaching lower elevation angles and tropospheric effects appear to dominate their respective measured pseudoranges causing the typical upward "tail" in the residual data. Ionospheric and clock drift effects are probable causes for the slopes of the residual curves. Ionospheric and tropospheric effects are discussed further in following sections.

(g) The major difference in the data from the two X-sets is the large offset in the X-set 1 data separating channels 1 and 3 from channels 2 and 4 as seen in Fig. 7. We have observed, on occasion, an inter-channel offset within an X-set that appeared to remain constant over the duration of a pass, but not from day to day. When observed in P-code data the exact value of the offset was not apparent. Offsets observed in C/A-code data, however, appeared to be a multiple of the 1 msec code length. In both cases, such an offset appeared to be related to an unpredictable internal timing error in one or more X-set channels.

(h) An estimate of the value of the interchannel bias in the X-set 1 data in Fig. 7 can be obtained by examining for all channels a subset of the ionospheric-corrected residual data from both X-sets corresponding to high

elevation angles, where tropospheric effects are minimal. If the large interchannel bias observed in X-set 1 was not present, then the average values over the subset interval, for each channel of the X-set 1 residual data, should all differ by the same amount from the corresponding average values for each channel of X-set 2. Figure 9 shows an hour-long period of ionospheric-corrected residual data from X-set 2 during which all satellites are above 20° in elevation. The average values for each channel are shown on the plot. The corresponding plot for X-set 1 is not shown here, but the average values were calculated for comparison with X-set 2, and for channels tracking the same signal on the two X-sets we see the following differences, in microseconds:

	Channel 1	Channel 2	Channel 3	Channel 4
X-set 1	-54.435	-54.043	-54.442	-54.005
X-set 2	-54.298	-53.374	-53.318	-53.359
Difference	- 1.137	- 0.669	- 1.124	- 0.646

(i) From these differences it can be seen that a net interchannel offset of approximately 0.5 μ sec existed in X-set 1 between channel pairs 1, 3, and 2, 4.

(j) An interreceiver offset or clock error does not affect position error in a navigation solution which includes solving for the user clock error; however, an interchannel offset does affect the user position. The navigation solution using the X-set 1 data in Fig. 7 is based on residual data containing an error between pairs of satellites of approximately 150 m (0.5 μ sec range equivalent). The effect of the interchannel offset will be seen in comparing the navigation errors from the two receivers.

(k) We have seen that direct comparison of the pseudorange residuals from X-set 1 and X-set 2 tracking the same signals is limited by biases between the receivers and biases within a receiver. It is meaningful, though, to remove biases and compare for a particular satellite, the pseudorange residual data as measured by each X-set. Figures 10 and 11 illustrate the Channel 1 (NAVSTAR 3) residuals measured by X-set 1 and X-set 2 after subtraction of the average value for each set of data so that each plot is centered around 0 μsec. The two sets of data visually show virtually the same shape and noise level. The spread of the data, as measured by the sigma in the statistical table on each plot, is based on a simple average; no attempt was made to perform higher order fitting on the data. The same results were found in comparing the other channels for each X-set after removal of the average values.

(2) Ionospheric Range Correction: The Channel 1 ionospheric range corrections at L1 which are shown, for each X-set, in Figs. 12 and 13 corresponding to the channel 1 pseudorange residual measurements of Figs. 10 and 11. The range corrections are plotted to the same vertical scale as the residuals so that the noisiness of the correction data over the residual data can be seen.

This will be discussed in a following section. An X-set-to-X-set comparison of the measured range corrections determined from the same signals shows that the shapes of the two sets of data, the noise levels, and the magnitudes are very nearly the same except for the corrections for X-set 2 having a slightly higher average value, even though there is a 25-minute gap in the data. It is possible that within the hardware of each X-set a small delay differential exists between the L1 and L2 signals, a delay that is unique to that X-set hardware, so that the two X-sets tracking the same L1 and L2 signals could measure a different magnitude of differential delay.

(3) Navigation Errors:

(a) The four sets of pseudorange residuals from each X-set can be corrected for ionospheric effects by subtracting the appropriate L1 range corrections; they can then be transformed into position or navigation errors. Figure 14 shows the navigation errors resulting from the ionospheric corrected X-set 1 pseudorange residuals and Fig. 15 shows the corresponding X-set 2 navigation errors. In comparing these two figures, the dramatic effect of the X-set 1 interchannel offset is obvious. The errors in latitude (LAT) and longitude (LONG), and the radial error ($RAD = \sqrt{LAT^2 + LONG^2}$) are shown.

(b) The magnitudes of the X-set 2 errors in Fig. 15 are representative of much of our navigation error data, but most other data have not been as flat over the duration of the pass. The observed longitude errors have been generally, over the early and midrange parts of the pass, between -25 m and 0 m, while the latitude errors are between -10 m and +10 m. Since the geometry repeats unchanged from day to day, the variations in curve shapes and magnitudes of ionospheric-corrected navigation errors are due to a number of other possible effects: troposphere, receiver interchannel offsets, clock errors, and ephemeris errors. No tropospheric corrections were attempted in this study, but observed effects are discussed in a later section. A gross interchannel offset has been observed to produce large variations in the navigation error; smaller offsets could also produce noticeable shape changes in the error curves.

(4) Conclusion: We have seen, in comparing the results of side-by-side tracking of the same signals, that interchannel biases exist within an X-set and affect the resulting navigation errors. The observed biases depended on the code used, but otherwise were unpredictable in magnitude and in the number of channels affected, and did not remain constant from pass to pass. These biases prevented comparison between X-sets in an absolute sense, but after removal of the biases it was meaningful to compare the pseudorange residuals from the same satellite signal for similarity of shape and noise level. In plotting the residual data after subtracting the average, we were able to see that the shape and noise level of residual data for corresponding channels of each X-set were virtually identical. For data corrupted by biases of known magnitude, such as in some C/A-code data, the biases could be removed and the results were found to be consistent with the same signal tracked on other days. In the case of P-code interchannel

biases of only approximately known magnitude, no attempt was made to remove any biases and, thus, the navigation errors could not be compared with unbiased data.

b. Comparison of P and C/A-Code Pseudorange Residuals and Navigation Errors: The direct comparison of P-code tracking and C/A-code tracking was accomplished on day 81.230 by assigning each X-set to track the L1 signal from NAVSTARS 3, 4, 5, and 6, with X-set 1 assigned to track the P code and X-set 2 the C/A code. When both X-sets were operational and it was possible to conduct side-by-side tracking on the X-sets for comparison of the two codes, the data in UFTIN block 8, containing the L2-L1 ionospheric delay measurements, were not recorded, so that simultaneous comparison of C/A and P-code data is possible only by using uncorrected P-code data.

(1) Pseudorange Residuals:

(a) The pseudorange residual data for NAVSTAR 4 as tracked on Channel 2 of each X-set are examined here. Figures 16 and 17 show the pseudorange residuals for the X-set 1 P code and the X-set 2 C/A code, respectively. The data are plotted on identical scales, and it can be seen that they have virtually the same shape; there are, however, three notable differences between the two sets of data:

(1) The average value of the Channel 2 C/A-code residual, as shown in the statistical table in Fig. 17, exhibits a large offset from the other channels. This is due to an apparent internal receiver timing error described earlier, wherein a large and unpredictable offset appears in one or more channels of the receiver. On this day, Channel 2 of X-set 2 has an average residual value of 3947.213 μ sec, while the other channels have values of about -53 μ sec. Noting that (3947.23 - 4000) μ sec = -52.77 μ sec, which is more in line with the other channels, it appears that the internal timing error for this day resulted in an offset of 4 C/A-code periods in the measured data. The 4 msec offset was subtracted out for plotting and calculation of navigation errors.

(2) The C/A-code data show a greater degree of tracking noise than the P-code data due to the difference in code clock

rates; the clock period defines the chip length or basic unit of resolution of the ranging code. The chip length of the C/A code (1/1.023 MHz) is 10 times greater than that of the P code (1/10.23 MHz) so that, assuming equal received power levels, the rms measurement noise of the C/A code should be on the order of 10 times greater than that of the P code. The two sets of data in Figs. 16 and 17 confirm this; and this observation was true of the remaining satellites, although the shapes were dependent on the particular satellite.

(3) At the end of the four-satellite pass interval, as NAVSTAR 4 was setting, its C/A-code data have anomalies not exhibited by the P-code data nor in any other satellite's data. These anomalies appear regularly at the same point in the pass every day, suggesting an effect related to the geometry of NAVSTAR 4 and the APL station. The effect appears in Fig. 17 as a discontinuity in the residuals, and it appears that as the satellite sets possible multipath interference is occurring. This is discussed in more detail in Section E.

(b) It was found that for a single X-set, comparison of residuals from the same satellite on different days showed that the shape and noise level changed very little on a short term day-to-day basis for whichever code was being tracked. This consistency on a single X-set was important when a hardware problem left only one operating X-set. It was possible to build a collection of many days of useful comparison data by tracking the L1 P codes, then the L1 C/A codes on alternate days with the remaining X-set. The basic relationship of the P-code and C/A-code residuals observed for simultaneous tracking on two X-sets, was also observed for the single X-set, alternating day method.

(2) Navigation Errors: The navigation errors resulting from the simultaneous P and C/A-code pseudorange residuals for day 81.230 are shown in Figs. 18 and 19. As with the residual data, the navigation errors for the two codes have the same basic shape and the C/A-code errors reflect the higher noise level of the C/A-code residuals.

(3) Conclusion: The P and C/A codes exhibit the same basic behavior as shown by comparing the shapes of pseudorange residual data for each code resulting from tracking the same satellite. The C/A code has a tracking noise level that is inherently higher than the P code; this expected noise level difference can be observed in both pseudorange residual data and the resulting navigation errors. A geometry-dependent anomaly is observed in the C/A-code data from NAVSTAR 4, suggesting possible multipath interference.

c. L2-L1 Ionospheric Measurements:

(1) The ionospheric delay introduced in the GPS navigation signals can be estimated by measuring the difference in arrival times of the L2 and L1 P codes from a satellite. At a given time, along a given path through the ionosphere, the group delay varies inversely as the square of the carrier frequency. The difference, $\Delta\tau$, between the group delays at L2 and L1 is caused by the frequency dependent ionospheric group delays τ_{GDL2}, τ_{GDL1}. The group delay at the L1 frequency is related to $\Delta\tau$ by:

$$\tau_{GDL1} = \Delta\tau \left[\left(\frac{f_{L1}}{f_{L2}}\right)^2 - 1\right]^{-1} \qquad (1)$$

so that a measurement of $\Delta\tau$ provides an estimate of τ_{GDL1} (Ref. 4). The value of τ_{GDL1} obtained from the $\Delta\tau$ difference measurement is referred to as the ionospheric range correction at L1. Figure 12 is a plot of the ionospheric range corrections for NAVSTAR 3 on day 81.233. The differential group-delay measurements are provided by the data processor at the same measurement times as the pseodurange data for each channel. A comparison of Figs. 10 and 12 demonstrates a noise level slightly higher on the ionospheric range correction data than on the L1 P-code residuals resulting from the fact that the differential delay is the difference between two measurements, each of which makes its own contribution to noise. If the L1 and L2 P-code tracking loop noise levels are equal, then the noise level of the pseudorange residuals after subtraction of the ionospheric range corrections is 3σ (Ref 5), where σ is the rms code loop measurement noise.

(a) Short Term Behavior:

(1) The effect of ionospheric range corrections is demonstrated by comparing the errors in Fig. 20, based on uncorrected residuals, with the errors in Fig. 21, based on ionospheric-corrected residuals. The noise level is greater in the plot of corrected errors as expected. The magnitude of latitudinal errors was reduced during the early and late stages of the pass as a result of the corrections, but remained unchanged during the middle portion; the

magnitude of the longitudinal errors was reduced only near the end of the pass, and to a lesser degree than the latitudinal errors.

(2) The change in magnitude of the corrected radial navigation errors is explained by considering the short term behavior of the ionospheric range corrections for all four satellites. Ionospheric correction consists of subtracting the scaled corrections from the appropriate pseudorange residuals. If the correction values for all satellites are the same at a point in time, subtracting that common value from each residual does not affect the magnitude of position error. If the correction values are not equal for all signals the position error magnitudes would reflect the differences in correction values among the four channels and the geometry at that time.

(3) The errors in Figure 21 are based on pseudorange residuals corrected with the ionospheric range corrections shown in Figure 22 for the four satellites. The data indicate different ionospheric effects on the satellite at the beginning and the end of the pass. Referring to the geometry plot in Figure 4, it can be seen that at the beginning of the pass (2300 GMT, 1800 EST), NAVSTARs 5 and 6 (with similar high correction values) are rising while NAVSTARs 3 and 4 are already at high (60°) elevation angles. At the end of the pass NAVSTARs 5 and 6 are still relatively high (30° and 50°) while NAVSTARs 3 and 4 are setting.

(4) An elevation angle dependence is observed on all four satellites; greater ionospheric delays correlate with lower elevation angles. This elevation angle dependence is consistent with the behavior of what is termed the ionospheric obliquity factor. The time delay along a nonvertical signal path can be estimated from the vertical delay at a point on the earth directly below the point where the signal path intersects the mean ionospheric height, taken to be 350 km. The vertical time delay, when multiplied by the obliquity factor, provides an approximation to the satellite-to-user delay. The obliquity factor, OF, is given (Ref. 6) by:

$$OF = \text{secant}\left(\sin^{-1}\left[0.948 \cos(E)\right]\right),$$

where

E = elevation angle.

(5) This factor varies from a value of 1 at 90° elevation to 3.14 at 0° elevation. User position errors due to this ionospheric effect are most significant when satellites, as seen by the users, are at different elevation angles. A single-frequency marine user might employ a simple elevation-angle test to determine when the difference in angles is likely to cause significantly different ionospheric effects on each signal and affect his position error.

(6) Comparing the corrections for NAVSTARs 5 and 6 as they rise at the beginning of the pass with those for NAVSTARs 3 and 4 as they set at the end, it can be seen that at very low elevation angles the magnitude of

the four measured delays are not equal. This behavior is compatible with the diurnal east-west gradient induced by the sun. NAVSTARs 5 and 6 are rising on this day approximately 6 hours past local noon to the west of APL and their signals are passing through a more active ionospheric region than the signals from NAVSTARs 3 and 4, three hours later, as they set to the south and to the east, respectively.

(7) If all four satellites were at approximately the same low elevation angle, a user's simple elevation angle test would not indicate ionospheric corruption of position, yet horizontal and temporal gradients could cause signals from different satellites to experience different ionospheric delays, which would increase a single frequency user's position error.

(b) Long Term Behavior:

(1) The measured ionospheric correction data show, for each satellite signal, an increasing magnitude over several weeks indicating increased ionospheric activity. Over the period of time for which we have ionospheric data the interval of time when all four satellites are visible shifted from evening to midday. For a given point on its trajectory, each satellite's signal passed through an ionosphere increasing in solar induced activity each day.

(2) This is demonstrated by comparing the ionospheric corrections for a single satellite, NAVSTAR 3, on two days (see Figs. 23 and 24), separated by 68 days. By selecting a fixed point on its trajectory defined by an elevation angle of 60 degrees and azimuth angle of 230 degrees, as an example, it can be seen that the correction value increased from approximately 40 nsec (66 minutes past 2300 GMT on day 81.233) to approximately 75 nsec (90 minutes past 1800 GMT on day 81.301). The satellite had come to the same point on its trajectory earlier by approximately 4 hours, 36 minutes (276 minutes).

(3) The ionospheric electron content and, thus, the ionospheric contribution to phase delay are directly affected by solar activity. The period of data collection (August to December 1981) was near the peak of the present 11-year solar cycle, a peak that was one of the highest on record (Ref. 7). During periods of lower activity, away from such a peak, the average level of the ionospheric electron content will be lower and differing ionospheric effects on each satellite's signal, which affect position error, should be reduced.

(c) Conclusion: The L2-L1 differential delay measurements from the X-set are consistent and offer apparently valid ionospheric corrections. The range correction curves exhibit reasonable behavior and have characteristics which might be explained by known ionospheric effects. A single-frequency marine user might benefit from using data only during those times when all satellites are high enough in elevation angle to minimize the differing ionospheric effects due to horizontal gradients and when all satellites are close enough together in elevation angle to minimize differing effects due to the elevation angle dependence of the electron content.

d. -Tropospheric Effects in Data:

(1) A signal passing through the troposphere, the atmospheric region extending to approximately 40 km above the earth's surface, experiences a frequency-independent phase delay due to the variation in refractive index. The effect has a functional dependence (Ref. 8):

$$D_t = CN(h) \text{ cosecant } (E) \qquad (2)$$

where C = constant of environmental conditions,

$N(h)$ = line integral of user to satellite refractivity function; a function of user altitude, h.

E = elevation angle of satellite.

(2) If the C and N(h) terms are constant during a pass, the variation in tropospheric delay is a function of satellite elevation angle only. The pseudo-range residual data for NAVSTAR 3 and 4 consistently take on a characteristic "tail", as the satellites set, and the corresponding navigation errors show the same effect as seen in Figs. 8 and 15. The cosecant of the NAVSTAR 3 elevation angle for the same pass on day 81.233 is shown in Fig. 25; the behavior of the residual data for NAVSTARs 3 and 4 correlates very well near the end of the pass with the elevation-angle dependence of the tropospheric effect.

(3) Tropospheric effects are well modeled (Ref. 9), and a marine user could reduce his navigation error when using low elevation angle data by incorporating a model, if he has available to him information about surface weather conditions such as temperature, relative humidity, and pressure.

e. C/A Code Multipath:

(1) The question of possible multipath in the C/A code signal arose due to the consisent anomalies in the NAVSTAR 4 C/A-code residuals as the satellite sets. It is known that a reflected signal can have a significant amplitude relative to the directly received signal. Both natural and man-made objects provide surfaces from which a signal can be reflected and then received (delayed in phase) simultaneously with the direct signal. Water is especially effective as such a surface. As NAVSTAR 4 sets almost due east of APL, the signal passes directly over some likely candidates for multipath reflection surfaces: the upper Chesapeake Bay, the Delaware Bay, and the Atlantic Ocean.

(2) A multipath signal will behave like noise of power equal to the direct signal if two conditions exist (Ref. 10):

(a) the receiver is already tracking the direct signal, and

(b) the delay difference, ΔT, in the reflected signal is greater than 1.5 code chips (1.5 μ sec for C/A code, 150 ns for P code).

The behavior of the NAVSTAR 4 residuals shown in Figs. 26 and 27, for days 81.217 and 81.302, is typical. The two sets of data were both taken by X-set 1, separated by 85 days; yet the "structure" of the residuals as the satellite sets is virtually identical for the two passes and does not have a noiselike character.

(3) The ground tracks of the satellites are fixed and the earth-fixed subsatellite point returns to a given point in its ground track about 4 minutes earlier each day. This means that the tracking geometry is identical from day to day, but occurs 4 minutes earlier. Figures 28 and 29 demonstrate the exact geometry of NAVSTAR 4 for the two days.

(4) The structure in the residuals consists of rapid (2-3 minutes) fluctuations of about 0.1 μ sec peak-to-peak magnitude (one-tenth of a C/A chip). The observed magnitude might have been greater if a data rate faster than 1 min. were used. The presence of a reflected signal with a differential delay of less than 1.5 μ sec would be within the range of the tracking loop which is, of course, already tracking the direct signal. A sufficiently powerful multipath signal could appear as coherent interference, causing the loop to respond to the sum of both signals until the received power of the reflected signal falls to a noninterfering level. The most severe effect on the tracking loop will occur when the reflected signal power is comparable to the direct signal power and the phase delay is large but within the range of the tracking loop.

(5) As seen in Fig. 27, the structure in the residuals exists from about 180 minutes past T0 until the satellite sets. The time history of the elevation and azimuth angles in Fig. 29 shows that the effect began when NAVSTAR 4 was approximately 9° in elevation and 80° in azimuth. Consider whether any of the large bodies of water east of APL could serve as a reflective surface for a multipath signal. If it is assumed that such a body of water can be treated as a horizontal, planar reflective surface, then the relationship between the reflected signal differential delay, ΔT; satellite elevation angle, θ ; user altitude, h; and the speed of light, c, is:

$$\Delta T = (2h\sin\theta)/c, \qquad (3)$$

and the horizontal distance between the user and the point of reflection is:

$$D = h\cot\theta. \qquad (4)$$

(6) If it is assumed also that the APL X-set antenna height of 100 meters above mean sea level places it at the same height (h = 100m) above one of

the water reflective surfaces considered above, it is possible to calculate both the theoretical differential delay and the distance from APL to the point of reflection when the effect first appears in the data at 9^{o} in elevation:

Elevation Angle	Distance, APL to Differential Delay	Point of Reflection
9^{o}	0.10 μsec	0.6 km

(7) The theoretical differential delay of 0.10 μ sec at 9^{o} is sufficient, if the reflected signal is strong enough, to interfere in the operation of the code tracking loop; however, the distance from APL to the point of reflection on the hypothetical surface, 0.6 km, is far short of ever the closest large body of water - the upper Chesapeake Bay, which is at least 40 km to the east.

(8) There are other possible sources of reflected signals to be considered: vertically oriented surfaces situated roughly on the opposite side of the X-set antenna from the satellite instead of horizontal surfaces between the antenna and the satellite. A signal reflected back onto the antenna from behind with power nearly equal to that of the direct signal and a phase delay of, say, 1 μ sec (300m path difference) is capable of causing the tracking loop to sense a shift of up to 0.5 μ sec in phase. Given the many structures in the APL facility, it is possible that one of these relatively large buildings or towers is the source of a reflected signal causing the observed affect on the C/A residual.

(9) Consider the case of a marine user with an antenna altitude of 15m, as an example. The maximum differential delay that can appear on a signal reflected from the surrounding water will occur when a satellite is directly overhead (sin 90^{o} = 1), and the reflected signal path will be greater than the direct path by twice the antenna height or 30m, producing a differential delay of 0.1 μ sec which is within range of the C/A code tracking loop. The differential delay decreases, as in Equation 3 above, as the sine of the elevation angle, so that any C/A-code multipath effects that a marine user might experience are likely to be most severe under conditions of calm seas and high elevation angle satellites.

(10) Conclusion: Geometry-dependent anomalies are observed in the C/A-code residuals from NAVSTAR 4 and multipath interference from a nearby structure is suspected. Any C/A-code multipath effects experienced by a marine user are likely to be most severe under conditions of calm seas and high satellite elevation angles.

4. CONCLUSIONS:

a. It was found that the P-code data uncorrected for ionosphere and the C/A-code data exhibit, as expected, the same basic characteristics with two exceptions:

(1) The C/A-code residual data are on the order of 10 times noisier than the P-code residual data. This is due to the factor of 10 difference between

the 1μ sec C/A-code chip length and the 100 ns P-code chip length. The noise level carries over into the navigation error domain, where just as with the residuals, the navigation errors of the P code exhibit the same basic behavior as the C/A-code errors.

(2) The C/A-code residual data for NAVSTAR 4 exhibit an anomaly as the satellite begins to set. At an elevation angle of about 9^{o} the data indicate that the tracking loop detects an interfering signal. The anomaly occurs in all the NAVSTAR 4 data that we have processed and appears to be geometry related. Without pursuing the problem in detail, we considered the most likely cause to be multipath, probably related to one of the large bodies of water to the east since the satellite sets due east of APL. Some simple calculations indicated that water related multipath was not probable; the most likely solution given the magnitude of the anomaly in the data, is reflections from a structure or structures in the APL Facility. Path differences of 30m. or more could result from reflections off nearby buildings or towers. An L1 C/A-code-only marine user, with an antenna height of 15m., as an example, could experience similar effects from water-reflected signals originating from a high-elevation angle satellite. The differential delay for such a reflected signal would be on the order of 1/10 C/A-code chip, which is within the coherent interference range of the tracking loop.

b. The dual frequency P-code phase-delay measurements available from the X-sets are found to provide a consistent and reasonable measure of the ionosphere. In comparing the navigation errors of P-code data uncorrected and corrected for the ionosphere, we find that the ionospheric effect, measured by the fixed-site APL facility, is most significant during the early and late parts of the pass when differences in elevation angles of the four satellites are most pronounced. A single-frequency user could benefit from an elevation-angle test identifying those parts of a pass most susceptible to elevation-angle dependent ionsospheric effects.

c. Interchannel biases within a receiver are neither constant nor predictable, but significantly affect user position error.

d. At low satellite elevation angles, tropospheric effects dominate the measured ranging data. Tropospheric effects are well modeled and a marine user could significantly reduce his navigation error when using low elevation angle data by incorporating a model if he has access to information about surface weather conditions such as temperature, relative humidity, and pressure.

5. REFERENCES.

1. R. J. Milliken and C. J. Zoller, "Principle of Operation of NAVSTAR and System Characteristics," Global Positioning System, Papers published in Navigation, The Institute of Navigation, Washington, D. C., pp. 12-14 (1980).

2. U.S.A.F., SAMSO/YEN, Computer Program Development Specification for the GPS X User Set (Unaided) of NAVSTAR GPS User Equipment Segment Phase 1 Configuration Item 330C 117, Specification Number CP-US-301. Code Ident. 12813, Part 1 of Two Parts, 20 Oct 1976.

3. A. J. Van Dierendonck, S. S. Russell, E. R. Lopitzke, and M. Birnbaum, "The GPS Navigation Message," Global Positioning System, Papers published in Navigation, The Institute of Navigation, Washington, D. C., p 59 (1980).

4. J. J. Spilker, "Signal Structure and Performance Characteristics,"Global Positioning System, Papers published in Navigation, The Institute of Navigation, Washington, D. C., p 35 (1980).

5. E. H. Martin, "GPS User Equipment Error Models," Global Positioning System, Papers publsihed in Navigation, Washington, D. C., p 116, (1980).

6. John A. Klobuchar, "A First-Order, Worldwide, Ionospheric, Time Delay Algorithm," AFCRL-TR-75-0502, Ionospheric Physics Laboratory, Project 4643, Air Force Cambridge Research Laboratories, Hanscomb AFB, Massachusetts, p 14 (25 September 1975).

7. Michael M. Feen, APL/JHU, Personal Communication.

8. E. H. Martin, op. cit., pp. 116-117 (1980).

9. H. D. Black, "An Easily Implemented Algorithm for the Tropospheric Range Correction," Journal of Geophysical Research, Vol. 83, No. B4, pp. 1825-1828 (1978).

10. J. J. Spilker, op. cit., p 53 (1980).

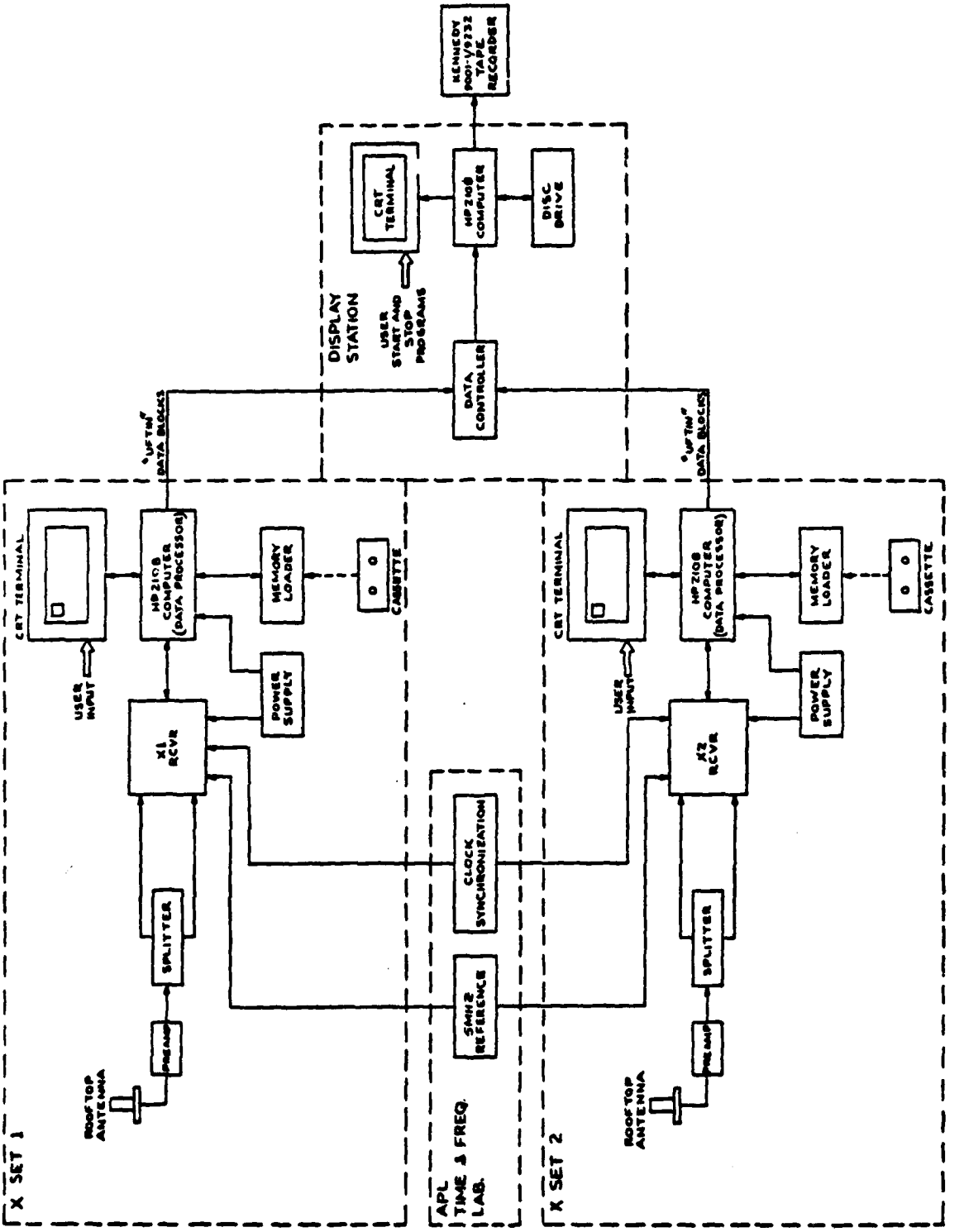

FIGURE 1. APL GPS MONITOR STATION.

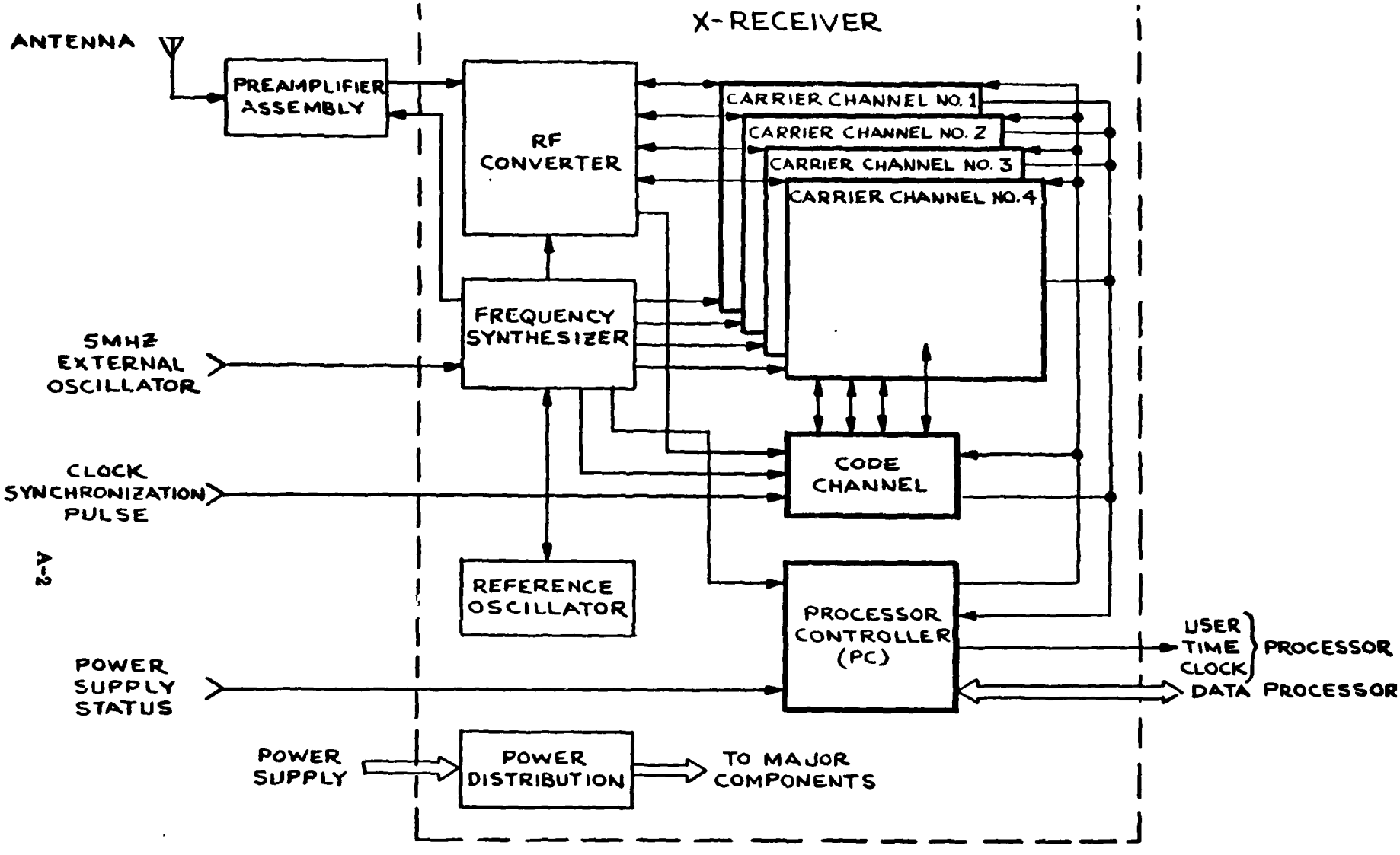

FIGURE 2. FUNCTIONAL BLOCK DIAGRAM OF X-RECEIVER MAJOR COMPONENTS.

X-SET BLOCK 6 X-SET 1

GPS TOW (D:H:M:S): 1:21:23:28.268

NAVT2: 159.5 SECS DATA INT: .7 SECS DR INT: .5 SECS

	CH 1	CH 2	CH 3	CH 4
HEALTH	010520	010462	010630	010420
C/F PSEUDORNG	177777 177022	177777 177025	177777 177011	177777 177020
C/F DELTARNG	000000 000002	000000 000001	000000 000001	000000 000001
CH QUALITY	000000	000000	000000	000000
SIG ASSIGN	000011	000011	000011	000011
RCVR QUALITY	100040			

FIGURE 3. DISPLAY STATION CRT SCREEN DISPLAY.

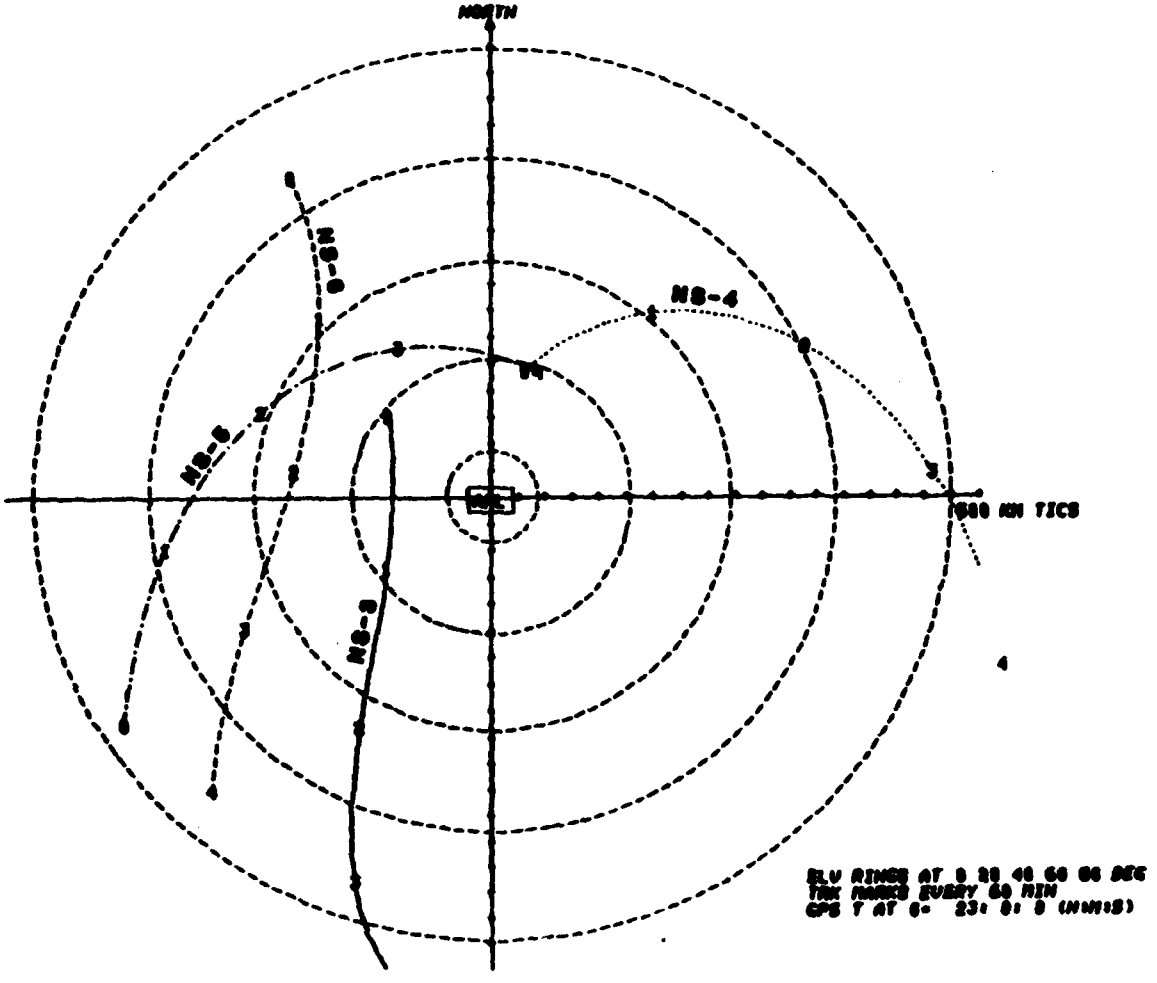

FIGURE 4. APL-CENTERED GROUND TRACKS; NAVSTARS 3, 4, 5, AND 6; DAY 81.233.

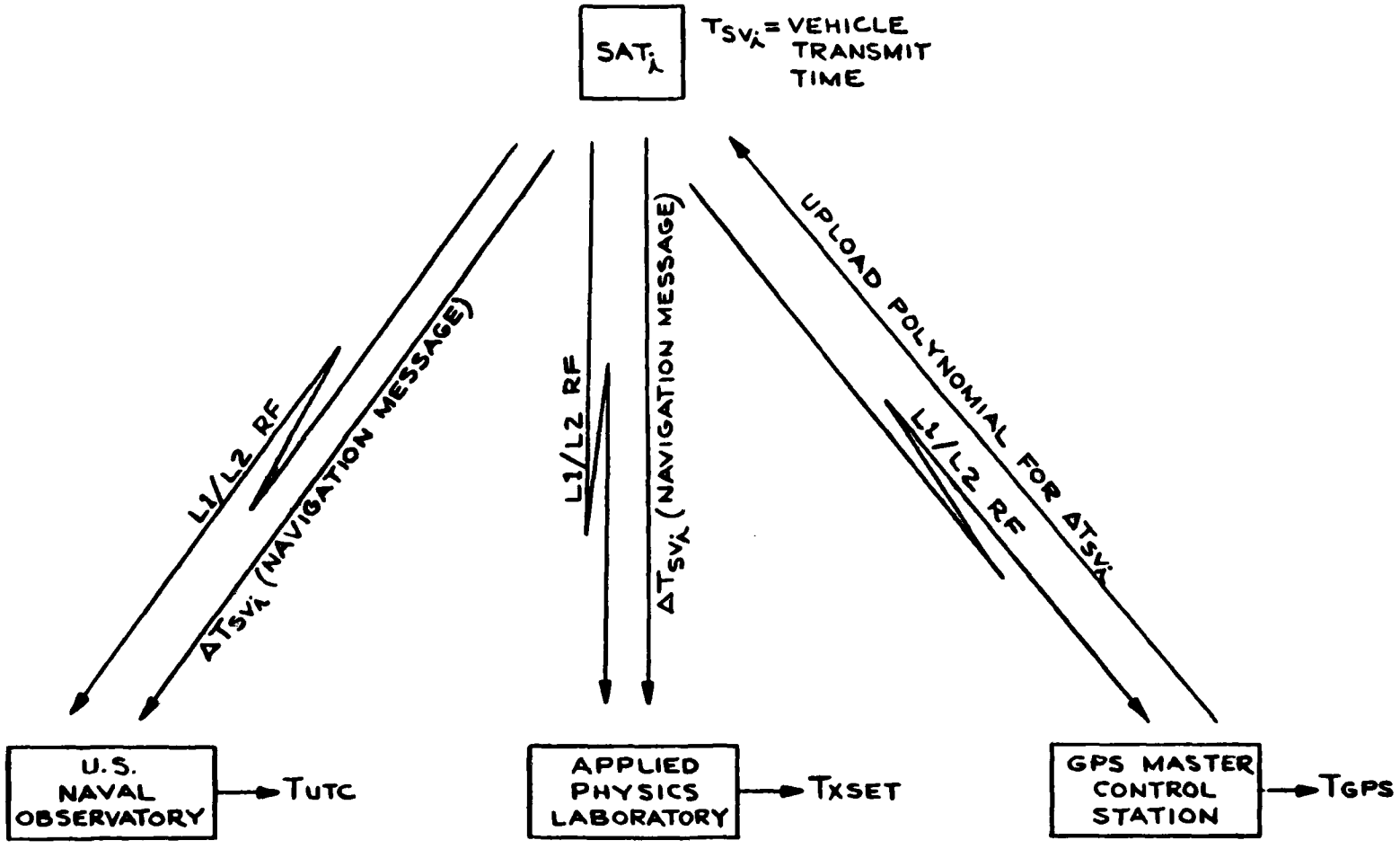

FIGURE 5. GPS SYSTEM TIMING.

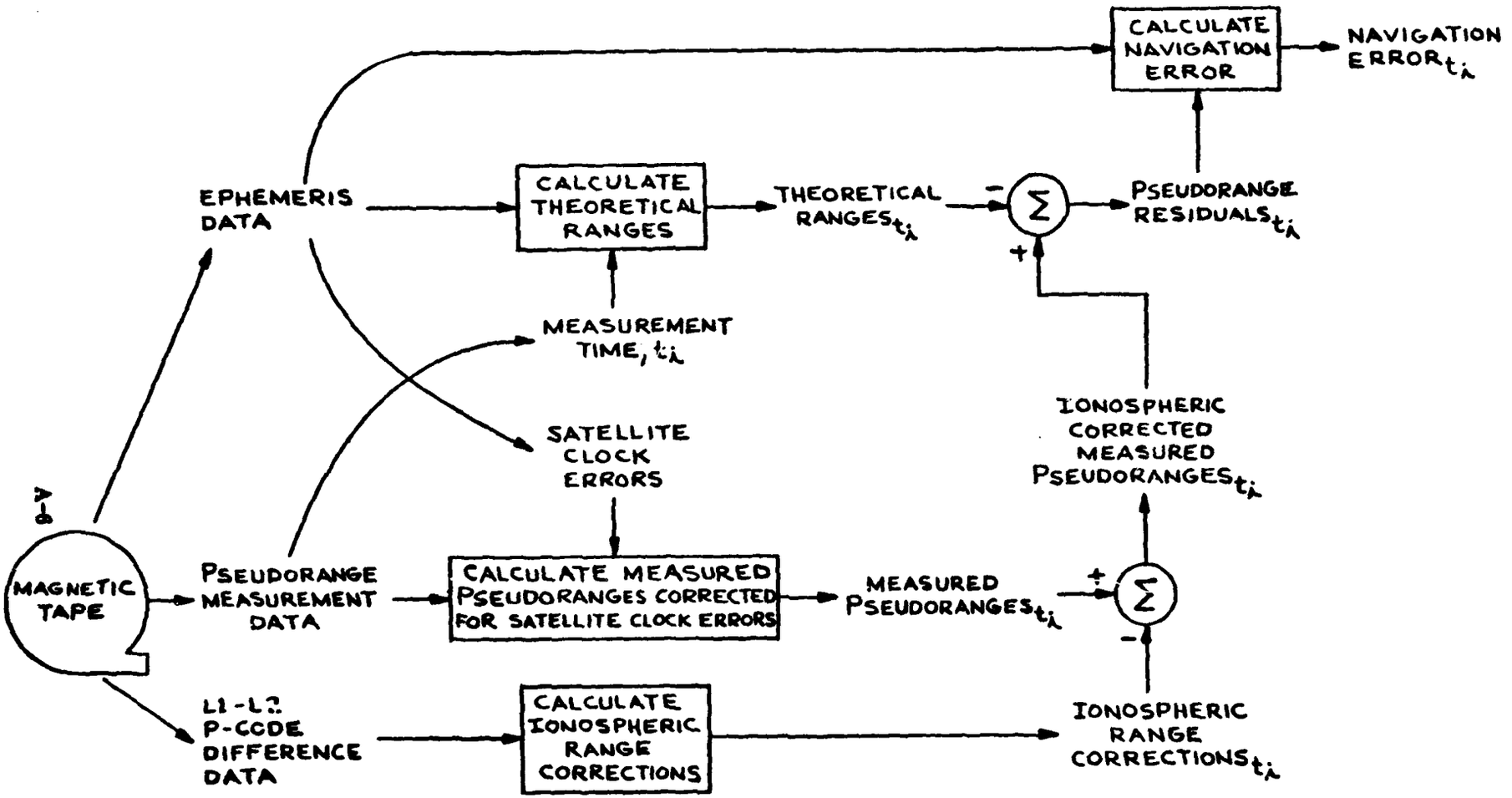

FIGURE 6. X-SET DATA PROCESSING FLOW.

NO REFRACTION CORRECTION

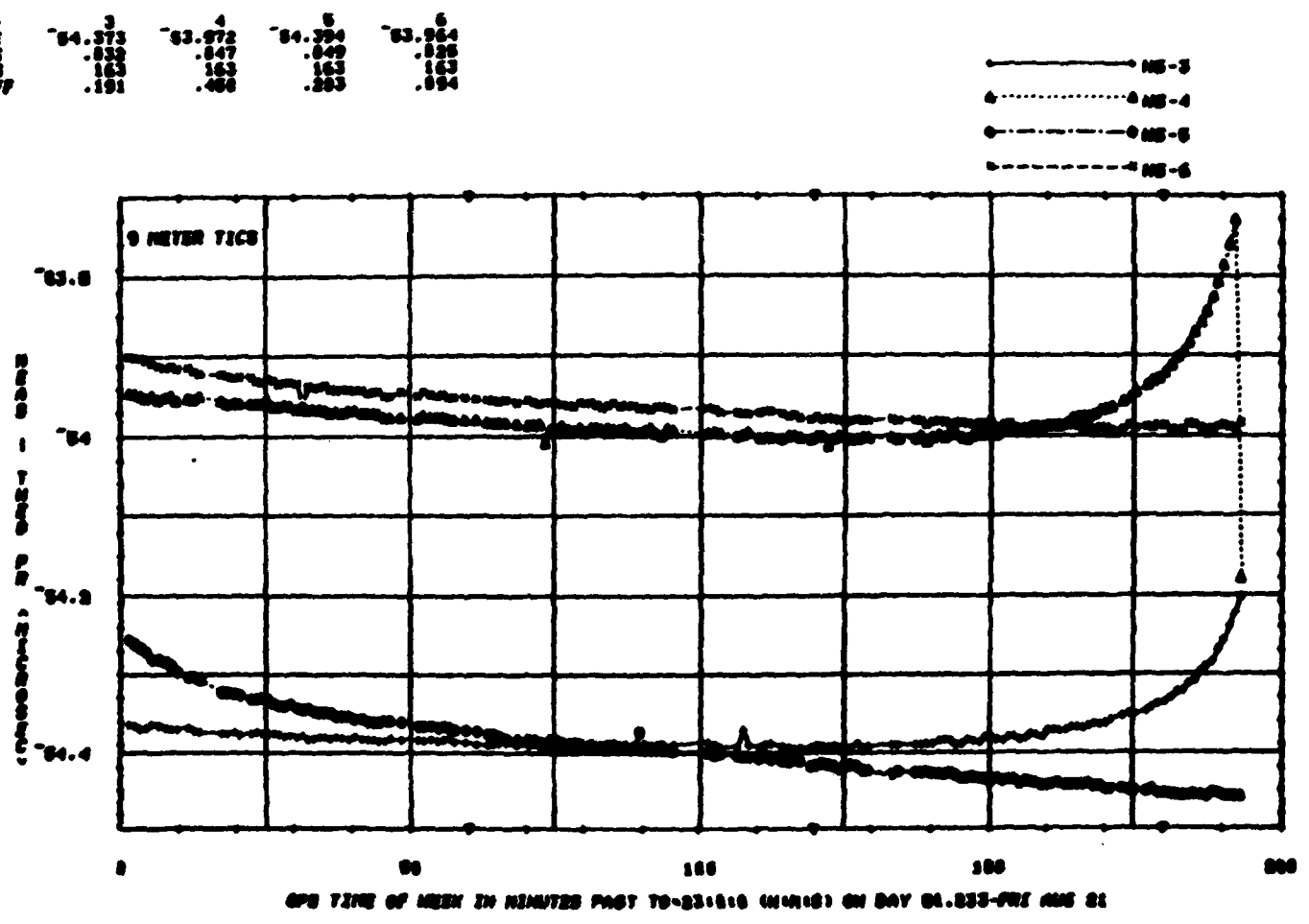

FIGURE 7. L1 P-CODE PSEUDORANGE RESIDUALS; X-SET 1; DAY 81.233.

NO REFRACTION CORRECTION

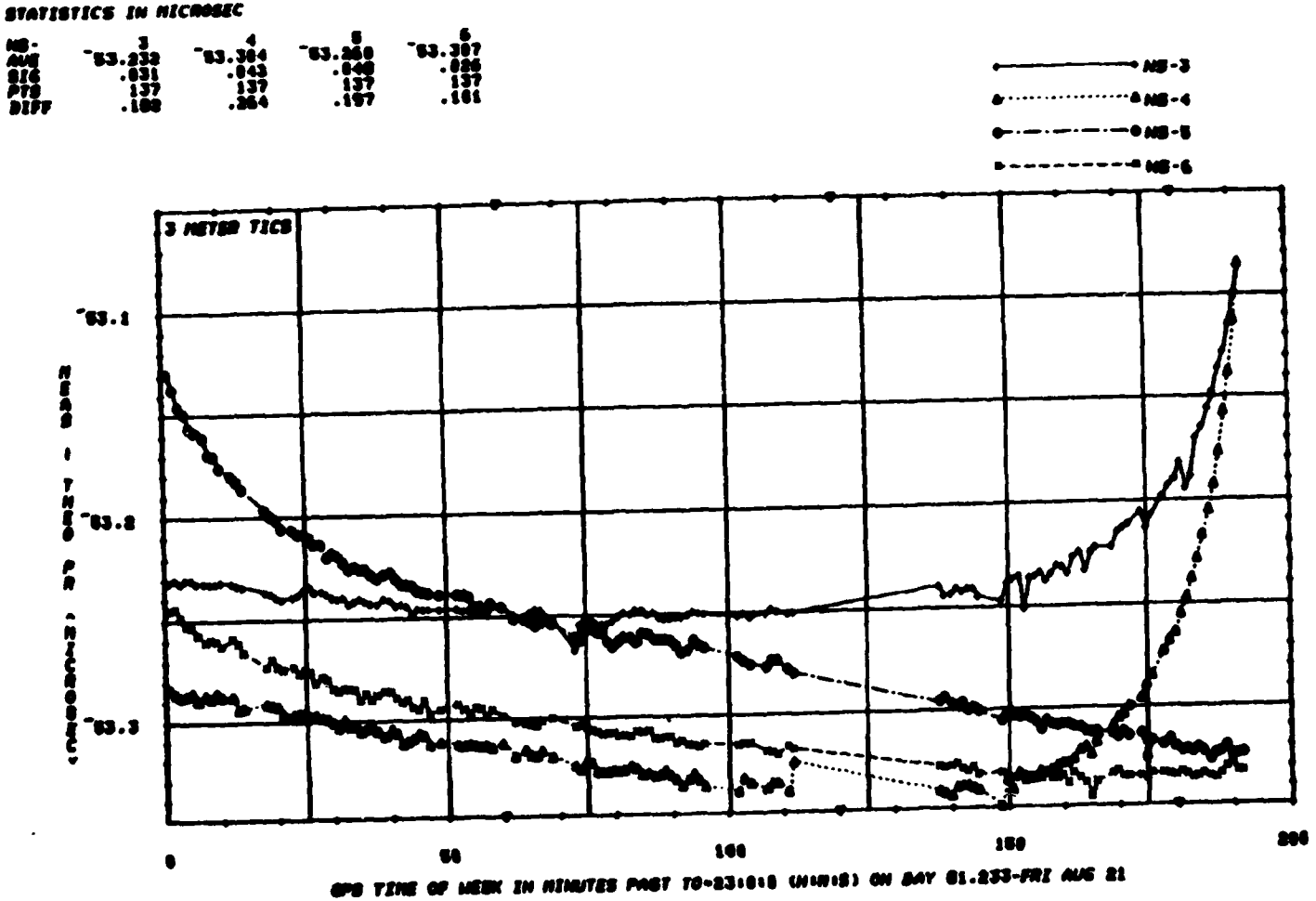

FIGURE 8. L1 P-CODE PSEUDORANGE RESIDUALS; X-SET 2; DAY 81.233.

REFRACTION CORRECTED

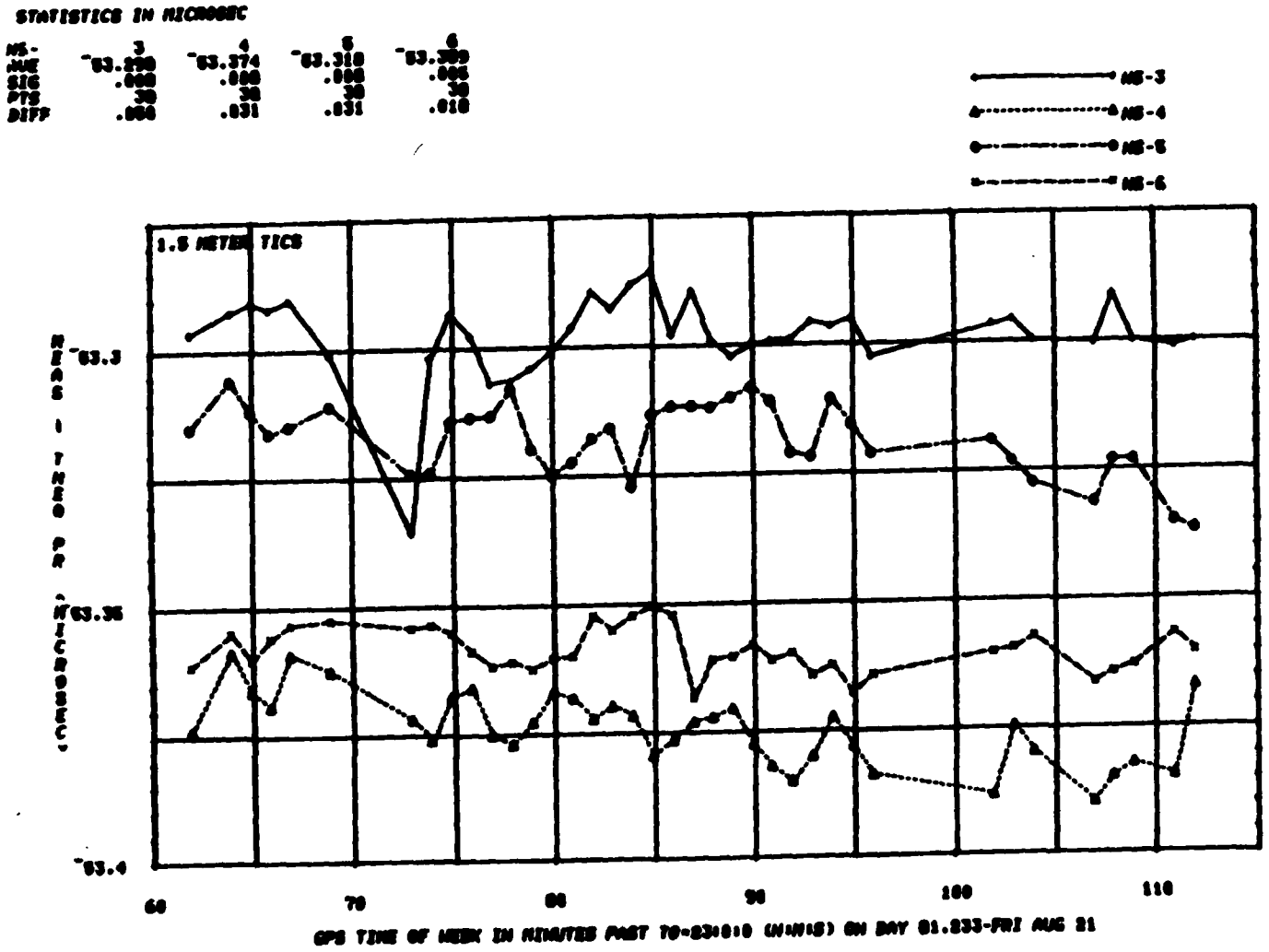

FIGURE 9. L1 P-CODE PSEUDORANGE RESIDUALS; X-SET 2; DAY 81.233; ELEVATION ANGLES $>20^{o}$.

NO REFRACTION CORRECTION

NS-	3	4	5	6
AVE	-84.373	-83.972	-84.384	-83.964
SIG	.832	.847	.849	.828
PTS	163	163	163	163
DIFF	.191	.468	.283	.094

STATISTICS IN NICROSEC

DATA PLOTTED FOR CHANNEL 1
AVERAGE SUBTRACTED FOR PLOTTING

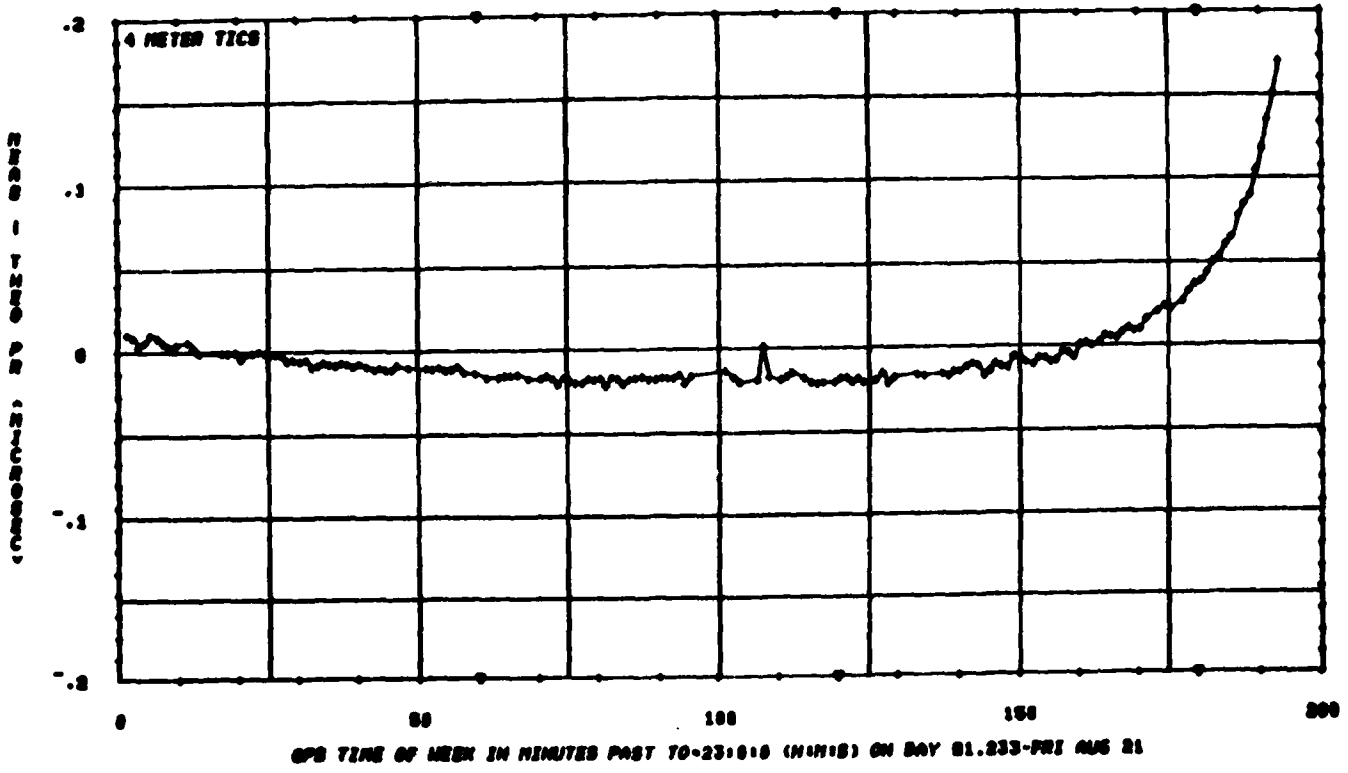

FIGURE 10. L1 P-CODE PSEUDORANGE RESIDUALS; X-SET 1; DAY 81.233; NAVSTAR 3.

NO REFRACTION CORRECTION

NB-	3	4	5	6
AVE	-53.232	-53.364	-53.260	-53.307
SIG	.031	.043	.040	.026
PTS	137	137	137	137
DIFF	.182	.264	.197	.101

STATISTICS IN NICROSEC

DATA PLOTTED FOR CHANNEL 1
AVERAGE SUBTRACTED FOR PLOTTING

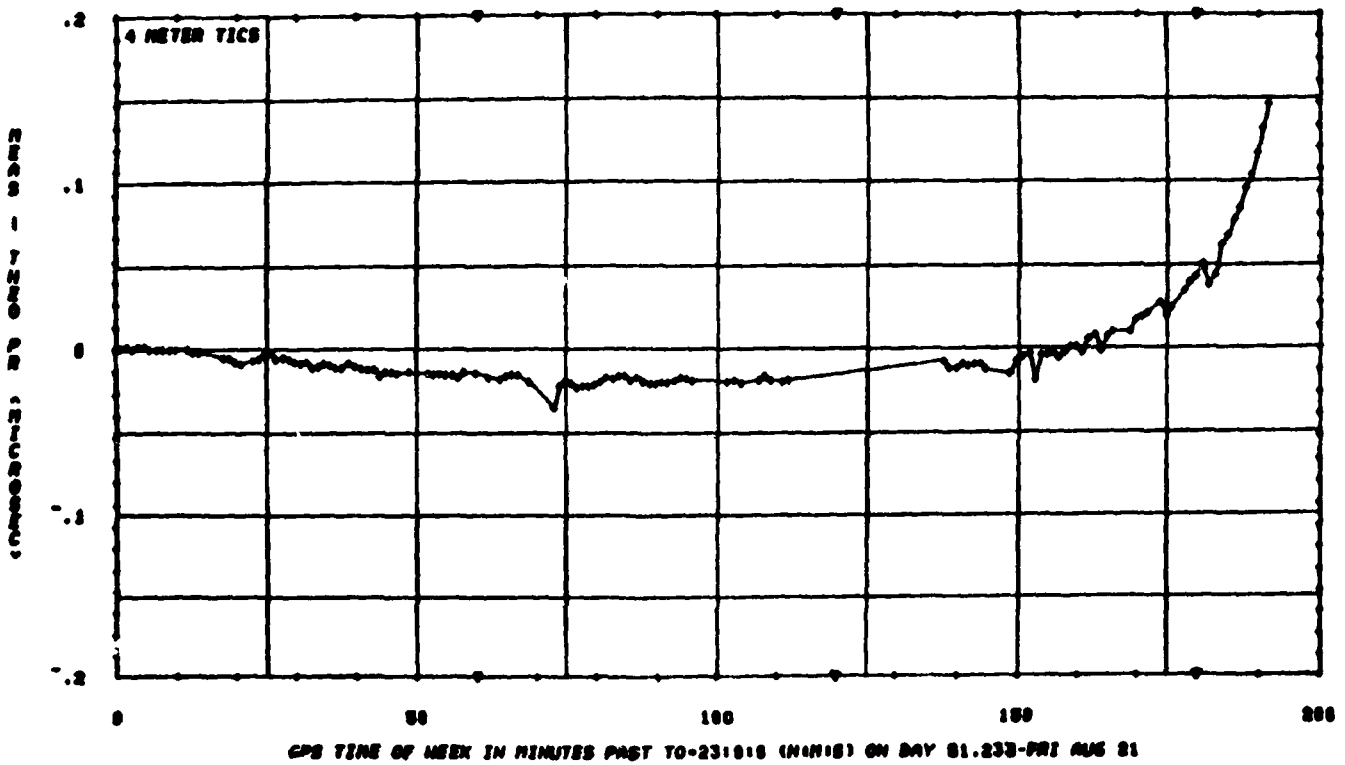

FIGURE 11. L1 P-CODE PSEUDORANGE RESIDUALS; X-SET 2; DAY 81.233; NAVSTAR 3.

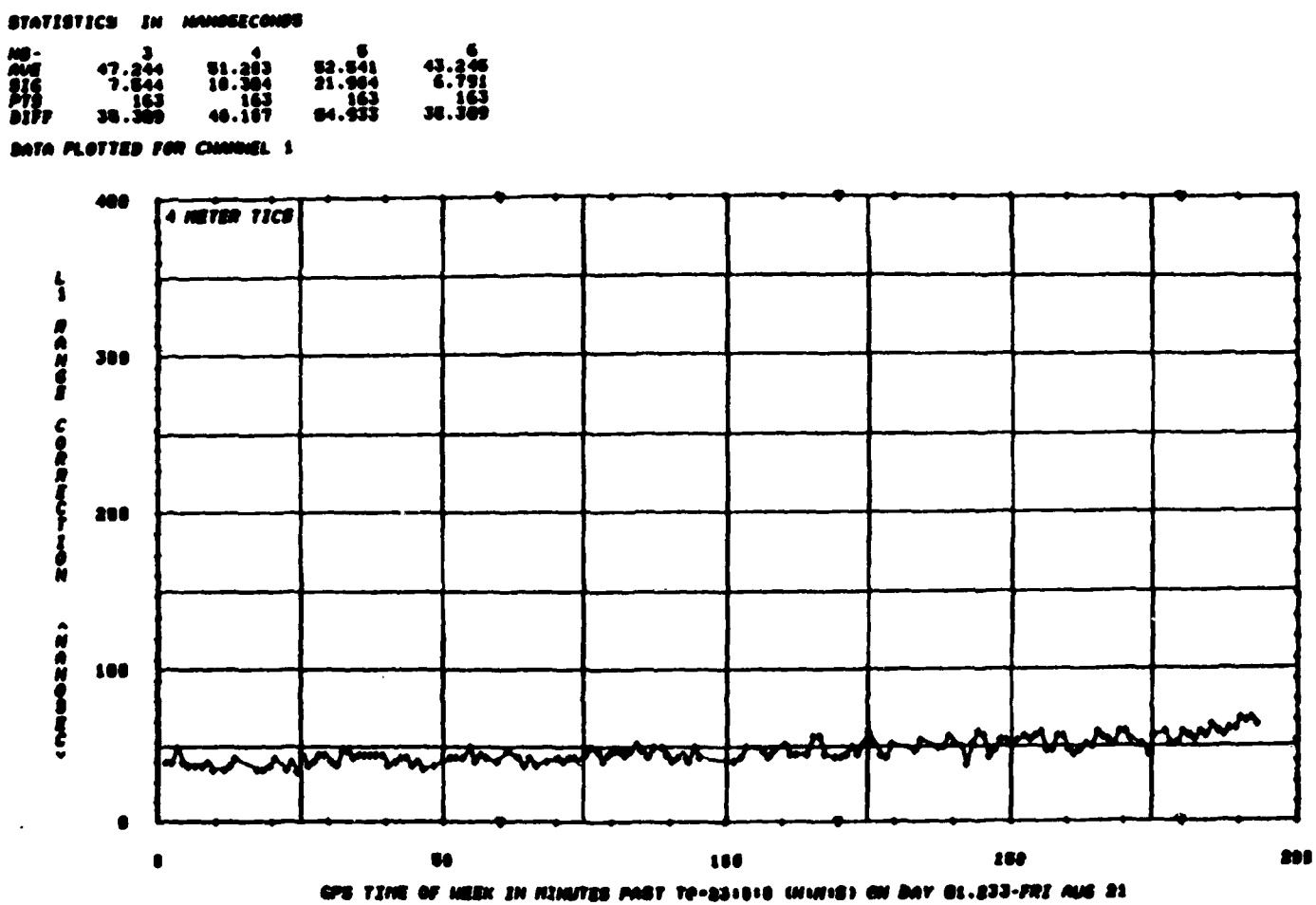

FIGURE 12. IONOSPHERIC RANGE CORRECTION AT L1; X-SET 1; DAY 81.233; NAVSTAR 3.

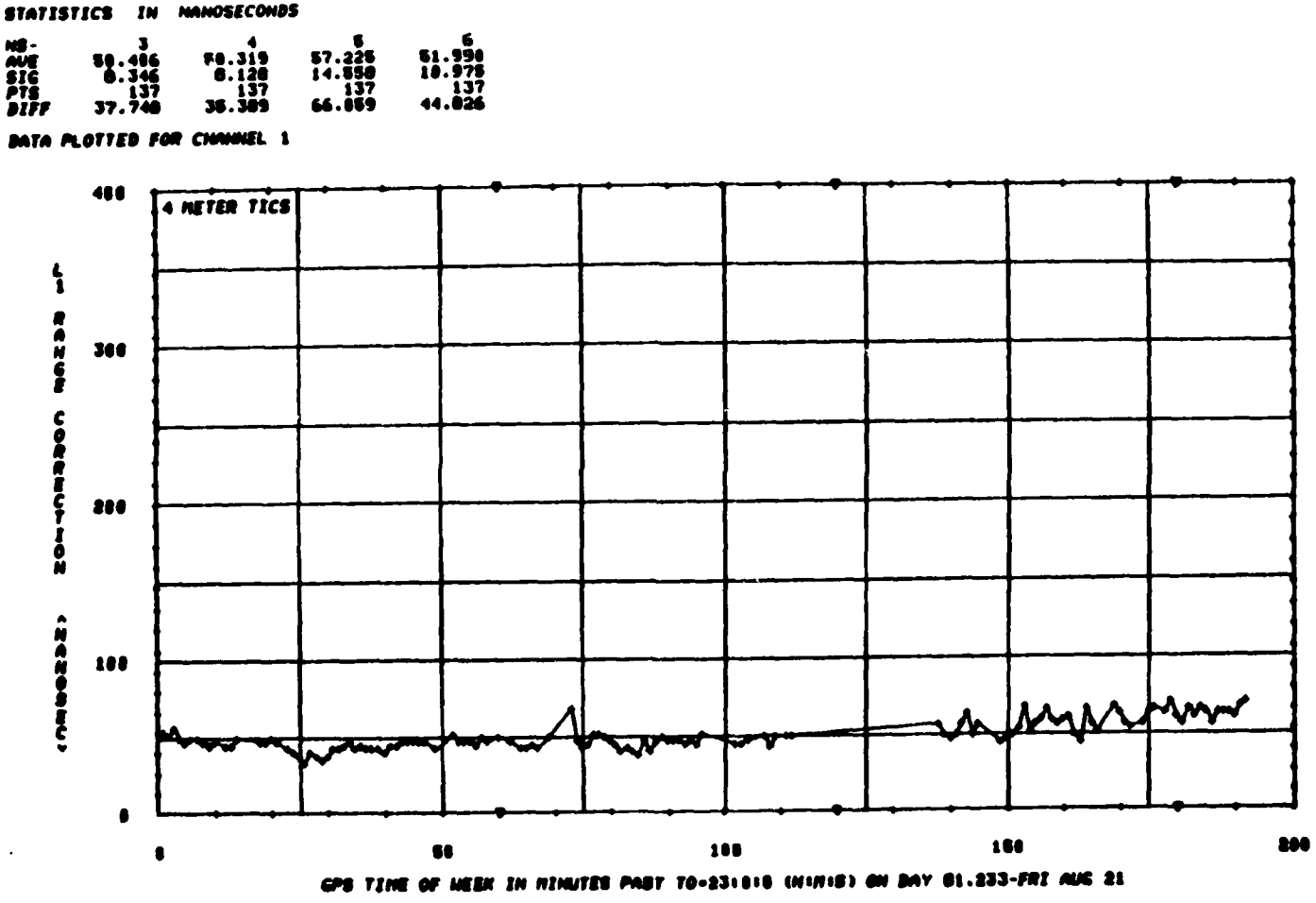

FIGURE 13. IONOSPHERIC RANGE CORRECTION AT L1; X-SET 2; DAY 81.233; NAVSTAR 3.

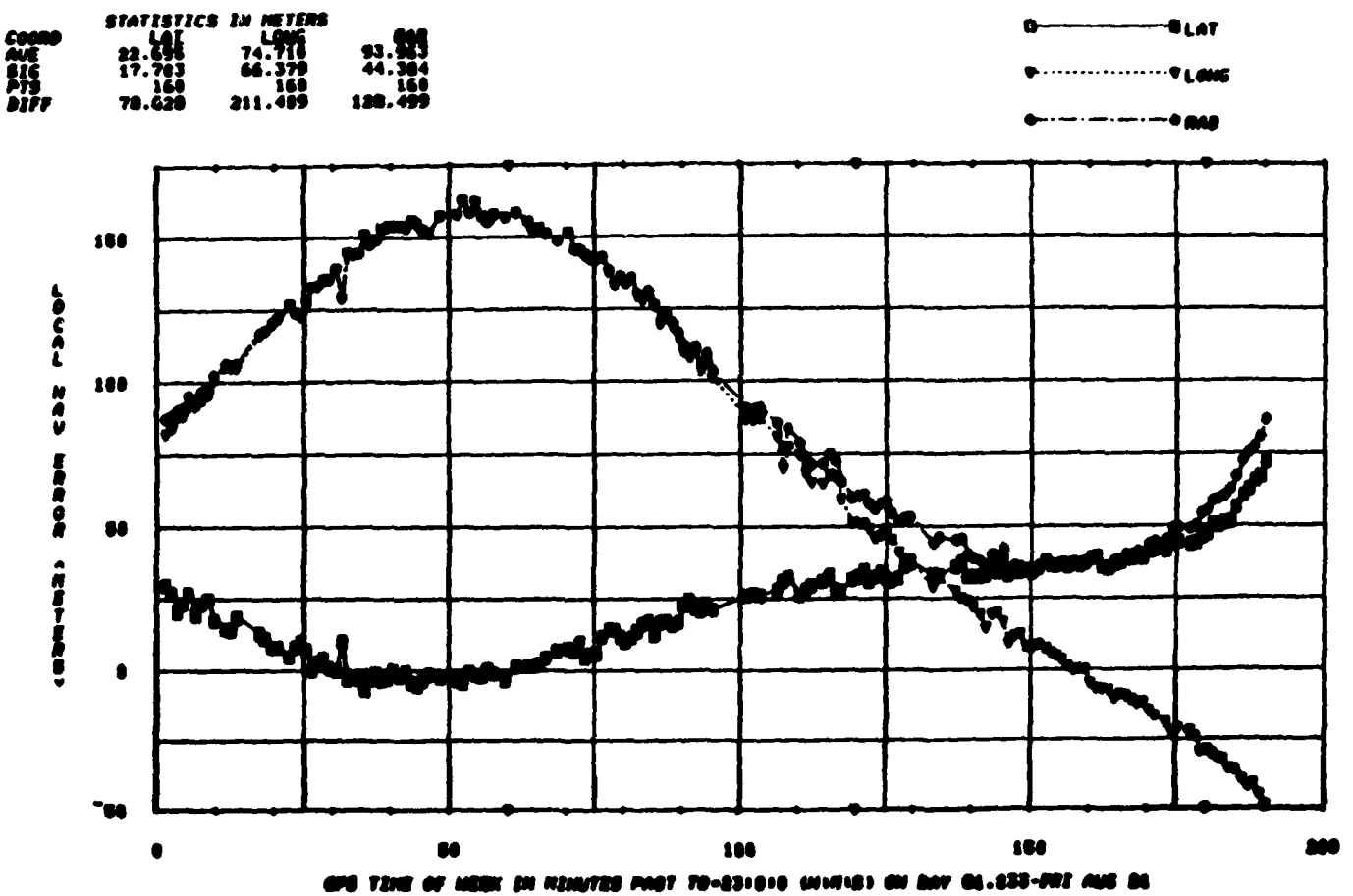

FIGURE 14. L1 P-CODE NAVIGATION ERRORS; X-SET 2; DAY 81.233.

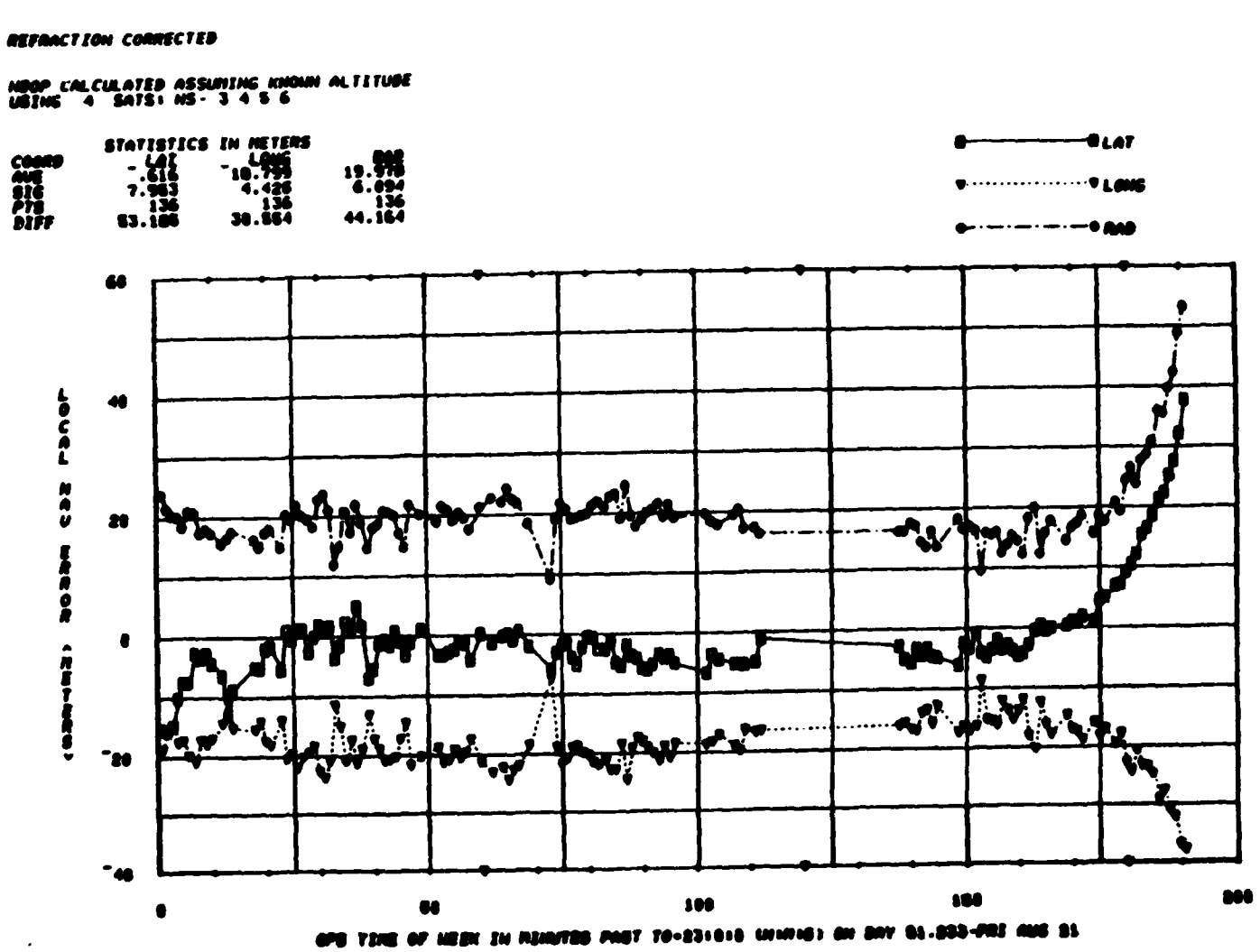

FIGURE 15. L1 P-CODE NAVIGATION ERRORS; X-SET 2; DAY 81.233.

NO REFRACTION CORRECTION

NO-	3	4	5	6
AVE	-83.196	-83.312	-83.284	-83.268
SIG	.823	.844	.846	.818
PTP	1.186	1.186	1.155	1.155
DIFF	.144	.284	.194	.074

STATISTICS IN NICROSEC

DATA PLOTTED FOR CHANNEL 2
AVERAGE SUBTRACTED FOR PLOTTING

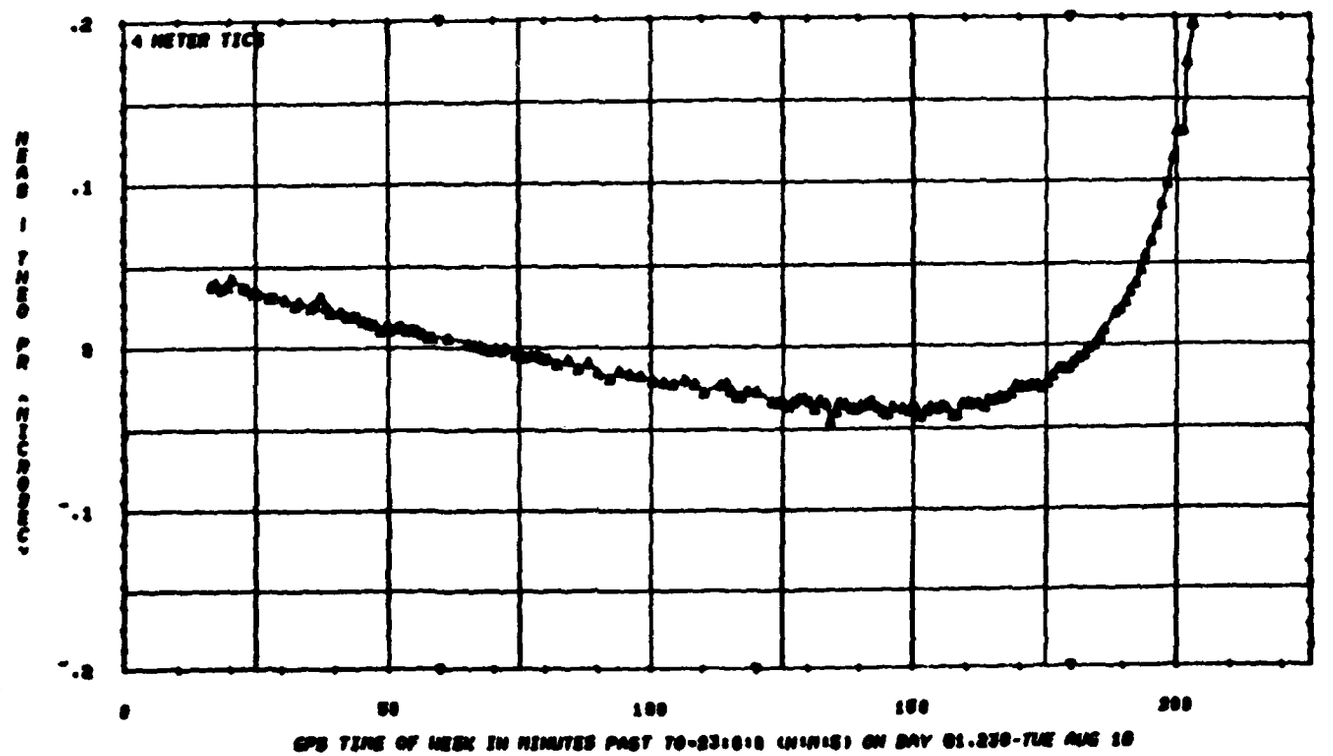

FIGURE 16. L1 P-CODE PSEUDORANGE RESIDUALS; X-SET 1; DAY 81.230; NAVSTAR 4.

NO REFRACTION CORRECTION

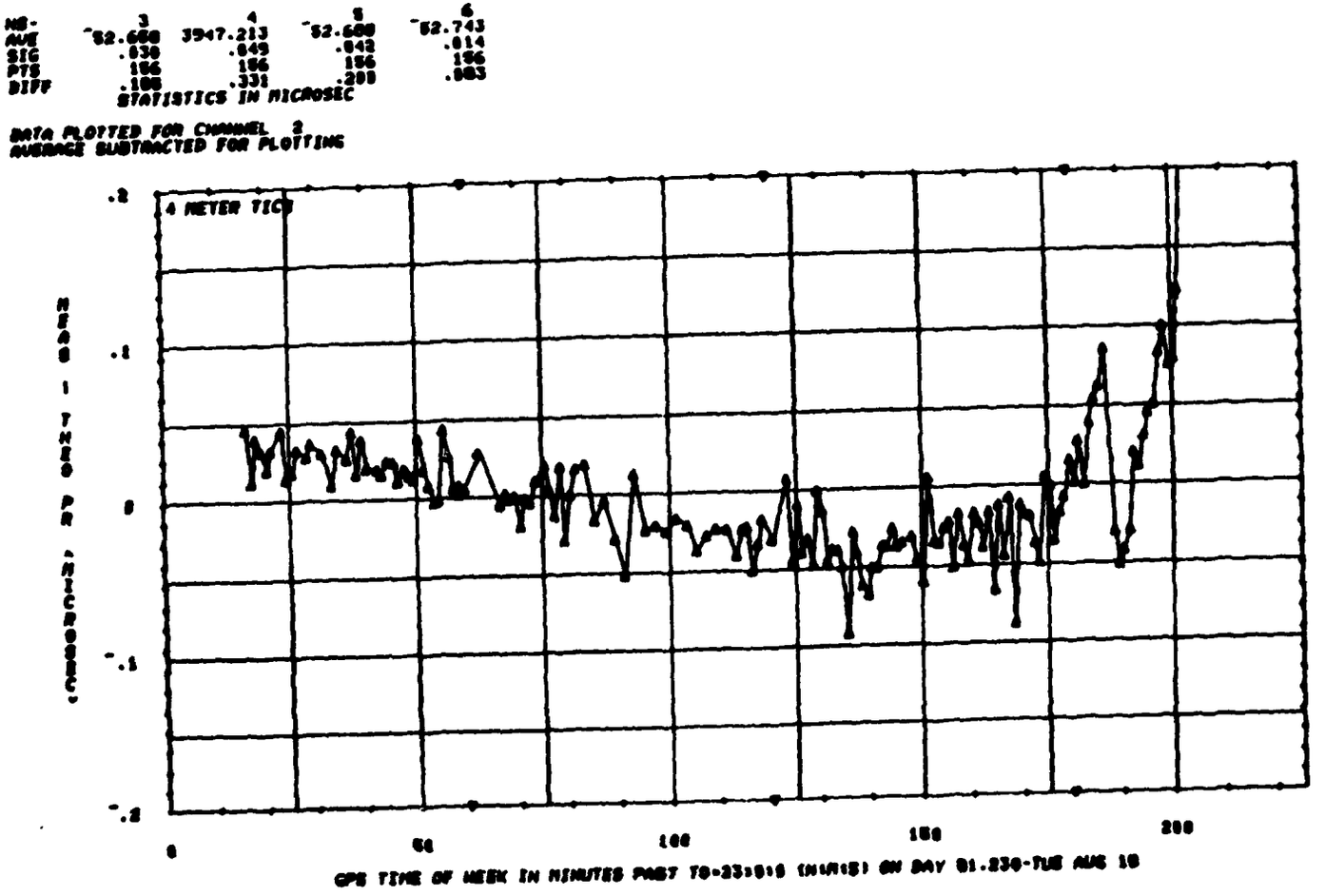

FIGURE 17. L1 C/A-CODE PSEUDORANGE RESIDUALS; X-SET 2; DAY 81.230; NAVSTAR 4.

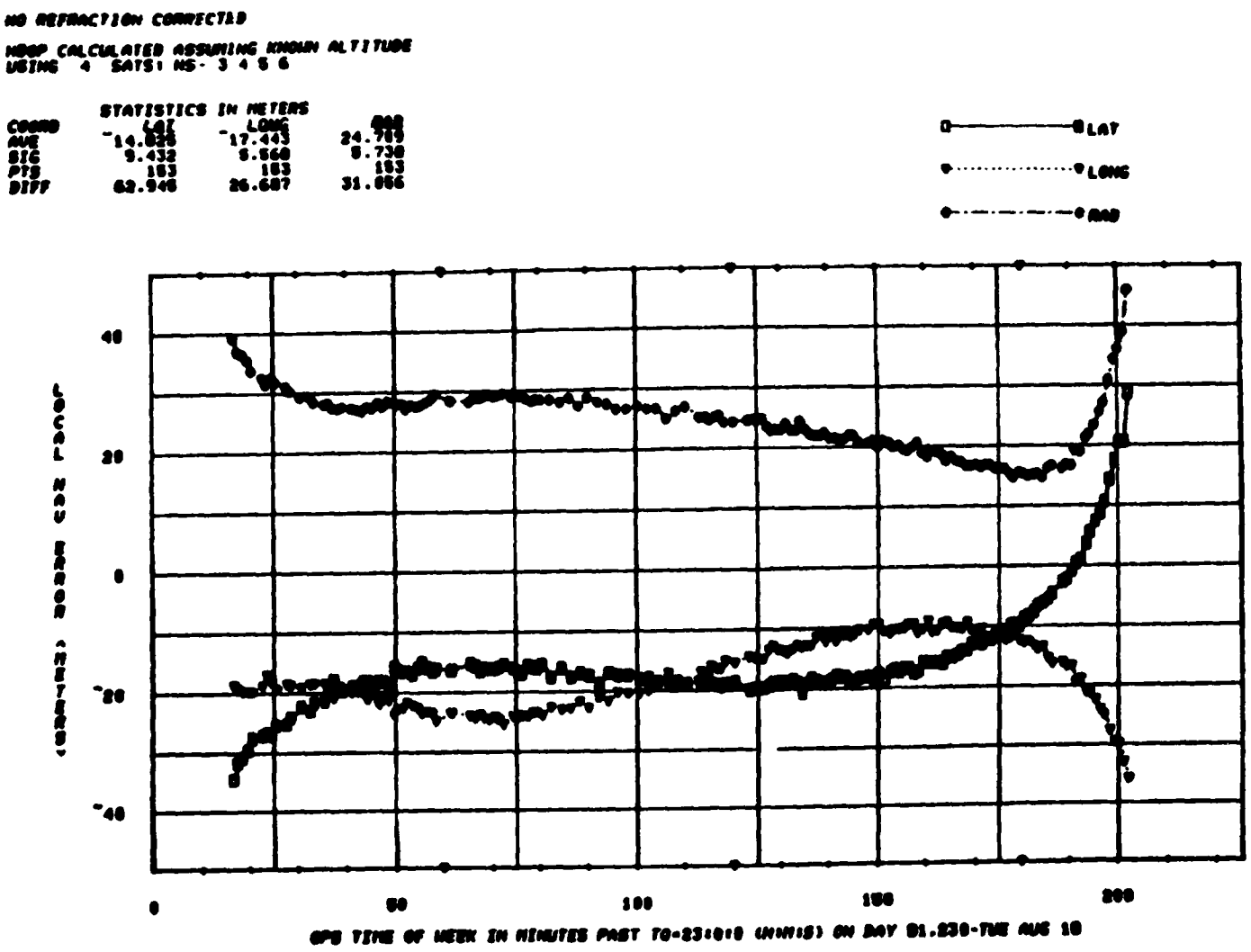

FIGURE 18. L1 P-CODE NAVIGATION ERRORS; X-SET 1; DAY 81.230.

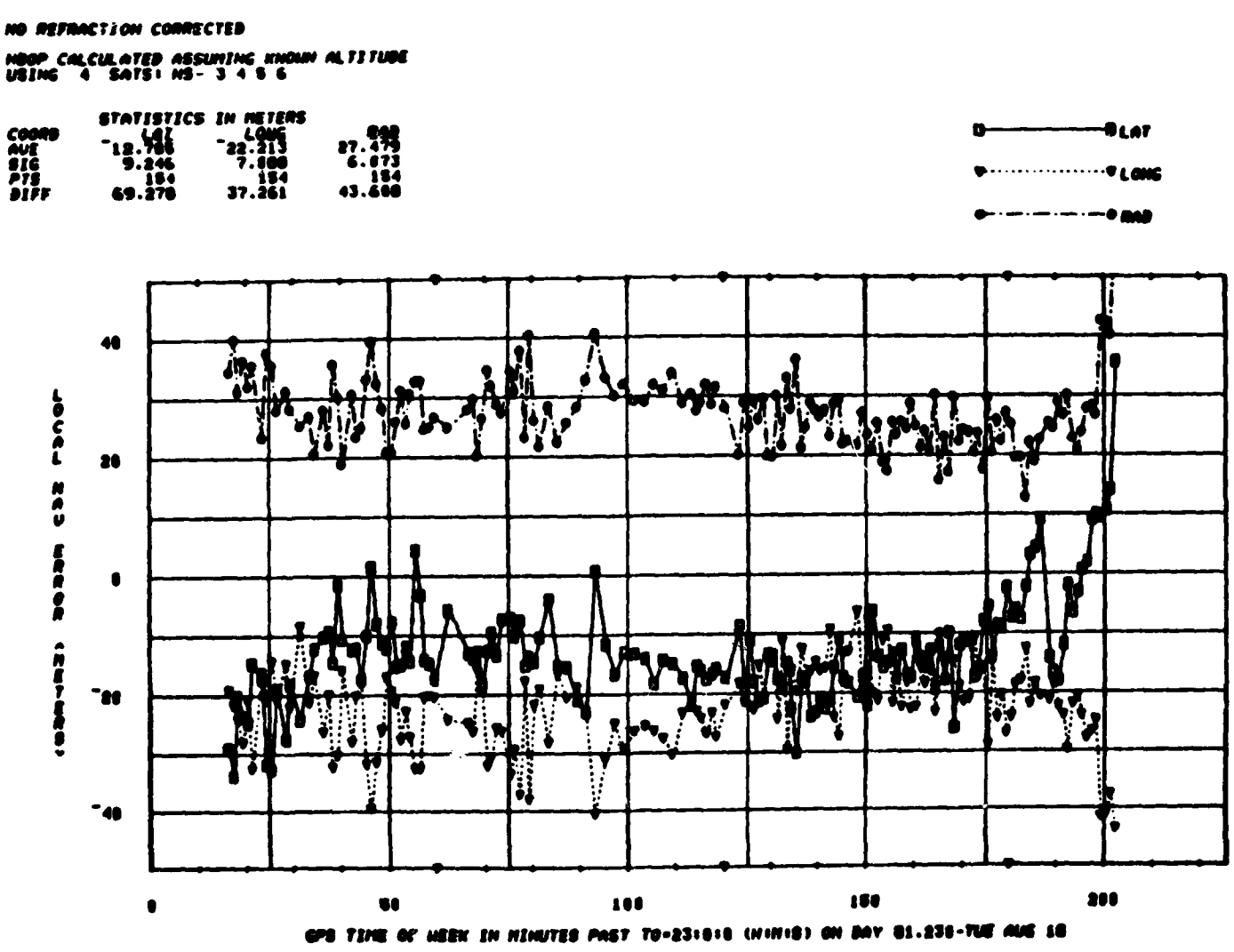

FIGURE 19. L1 C/A-CODE NAVIGATION ERRORS; X-SET 2; DAY 81.230.

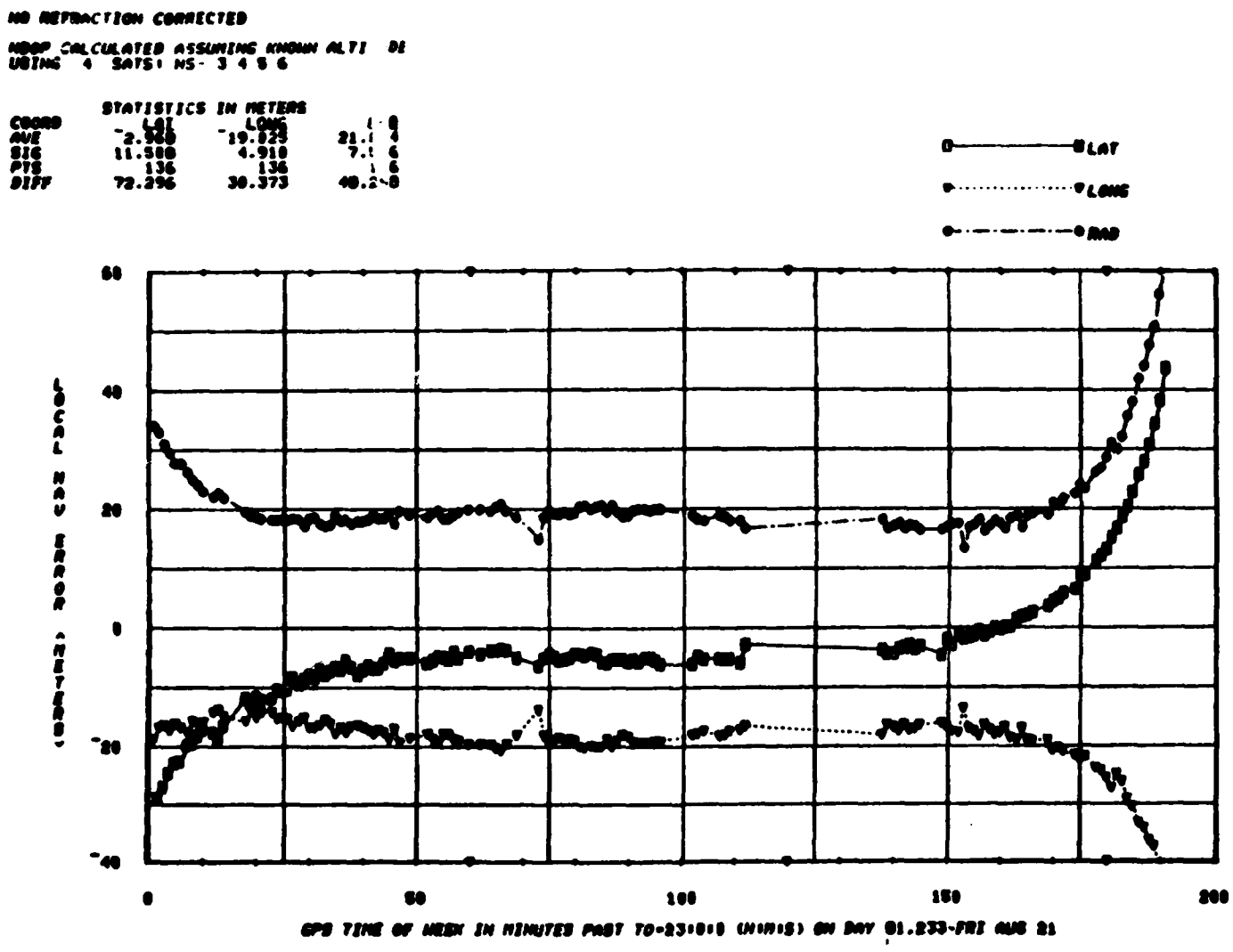

FIGURE 20. L1 P-CODE NAVIGATION ERRORS; X-SET 2; DAY 81.233.

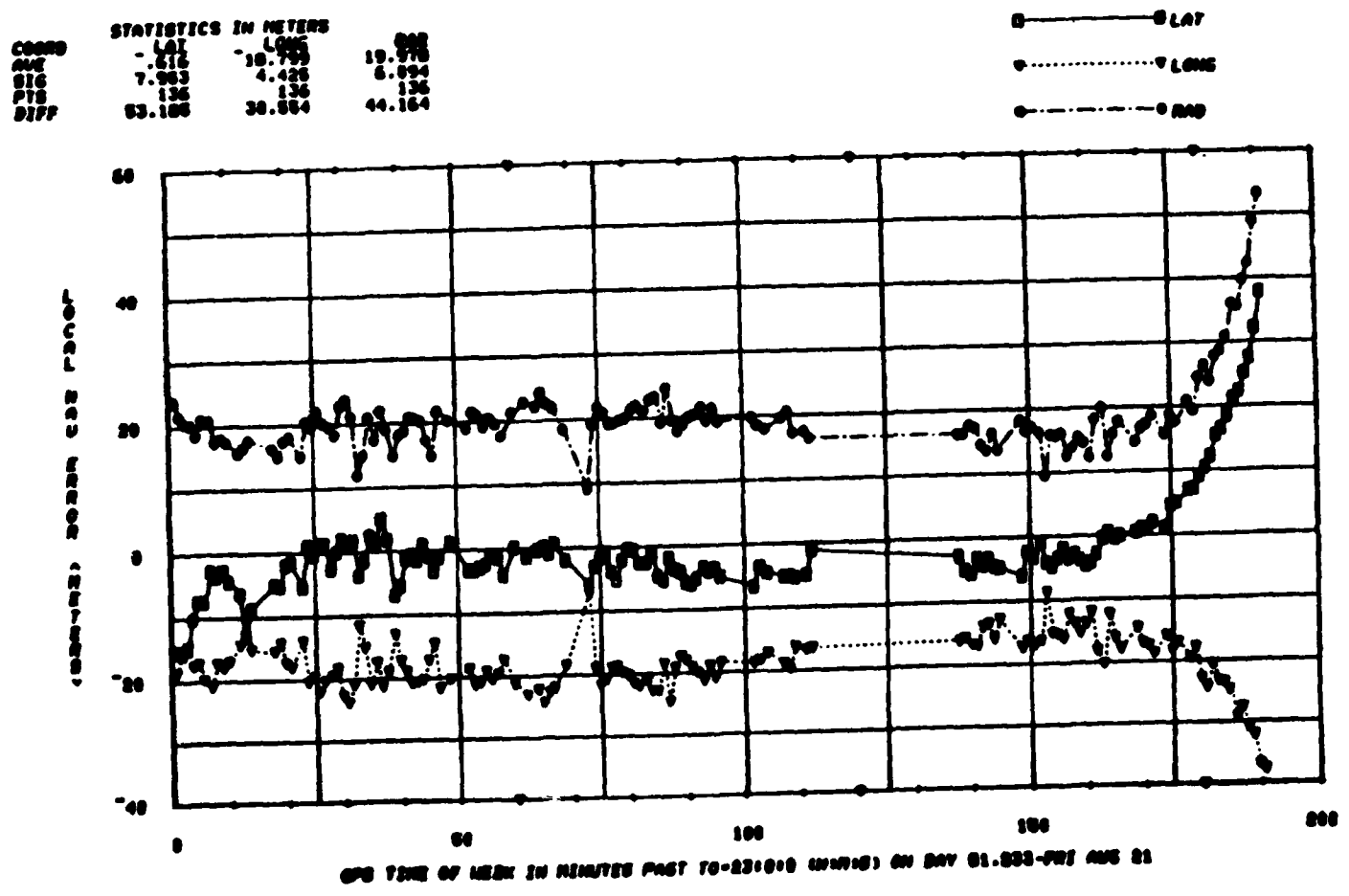

FIGURE 21. L1 P-CODE NAVIGATION ERRORS; X-SET 2; DAY 81.233.

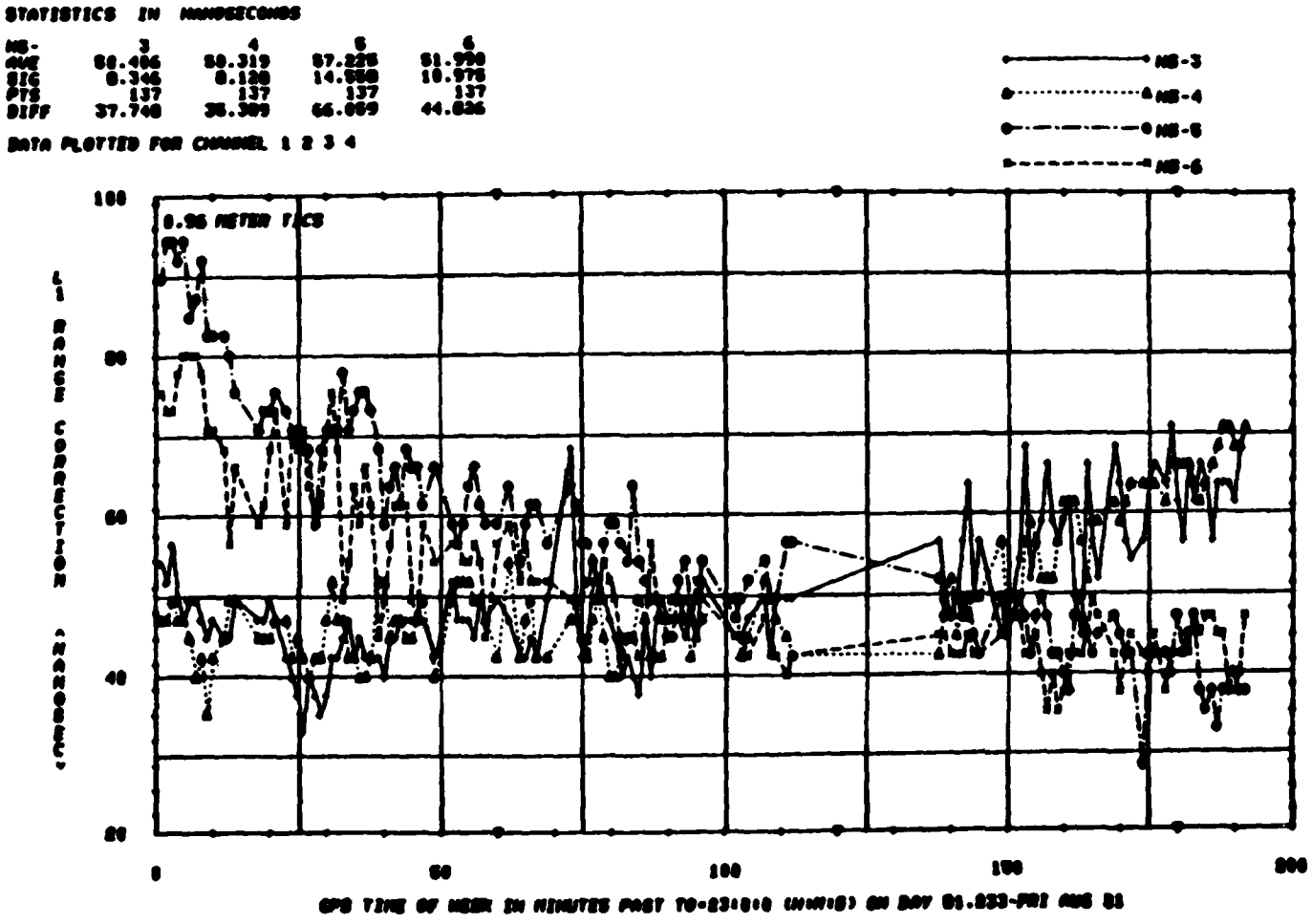

FIGURE 22. IONOSPHERIC RANGE CORRECTION AT L1; X-SET 2; DAY 81.233; NAVSTARS 3, 4, 5, AND 6.

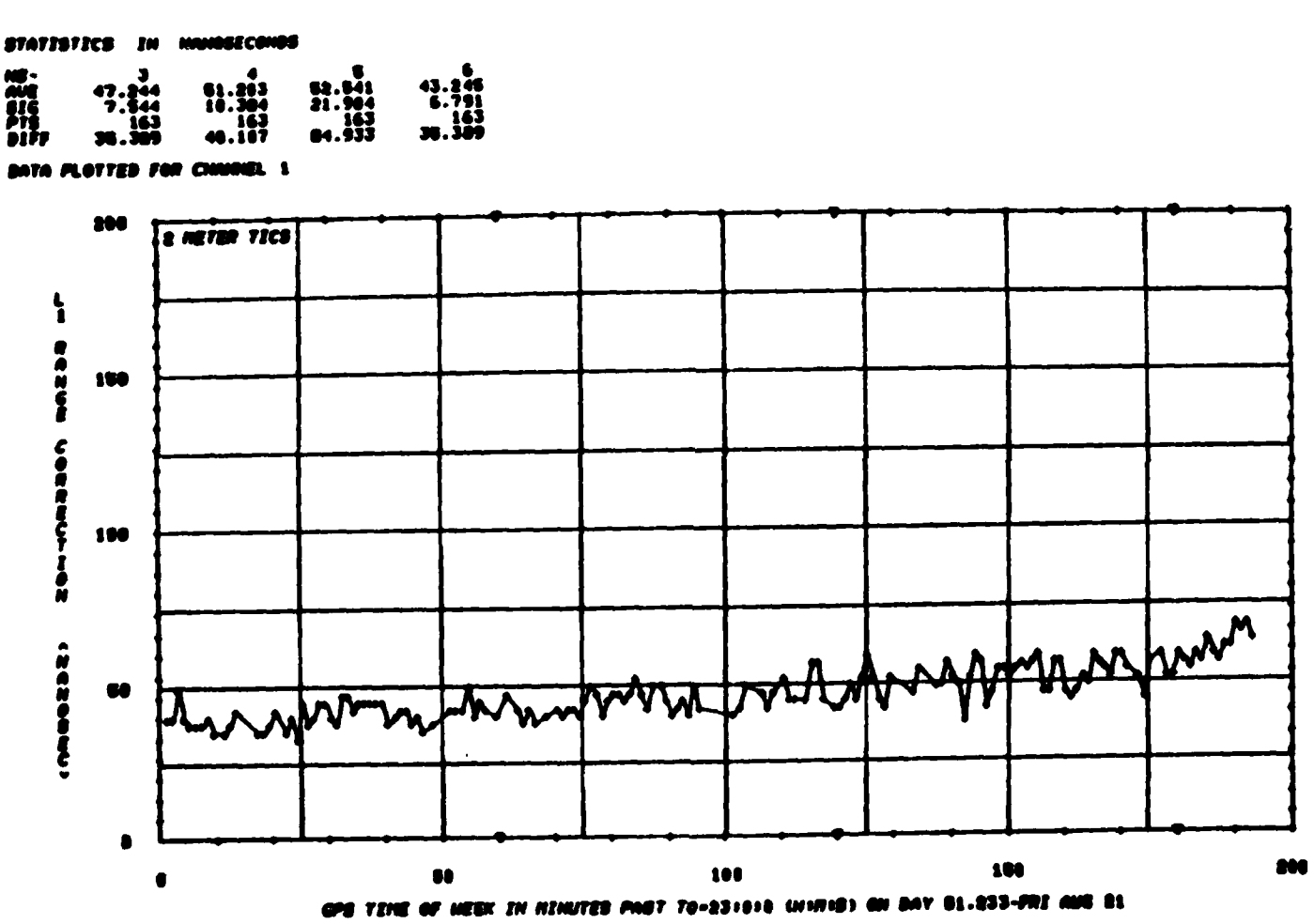

FIGURE 23. IONOSPHERIC RANGE CORRECTION AT L1; X-SET 1; DAY 81.233; NAVSTAR 3.

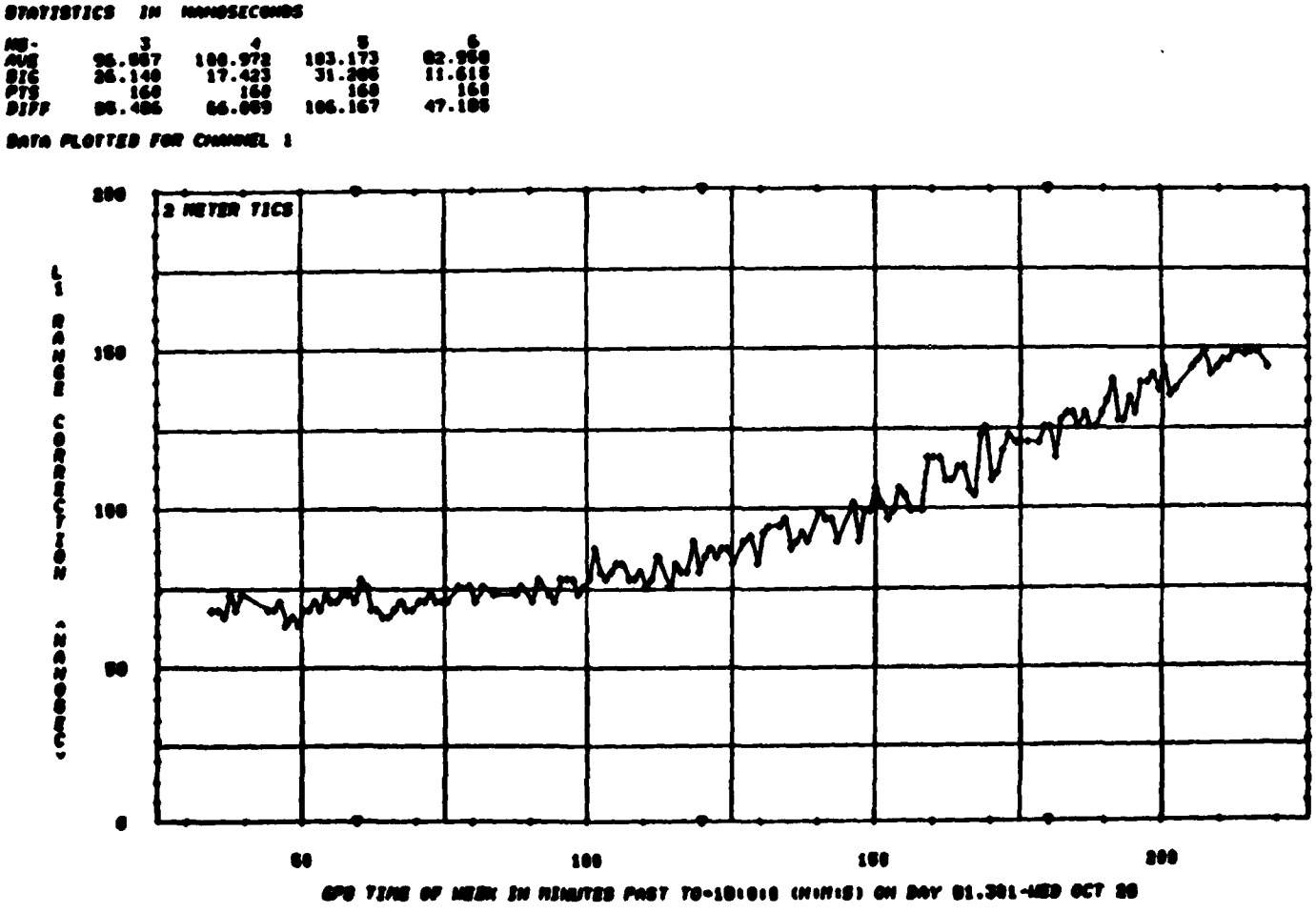

FIGURE 24. IONOSPHERIC RANGE CORRECTION AT L1; X-SET 1; DAY 81.301; NAVSTAR 3.

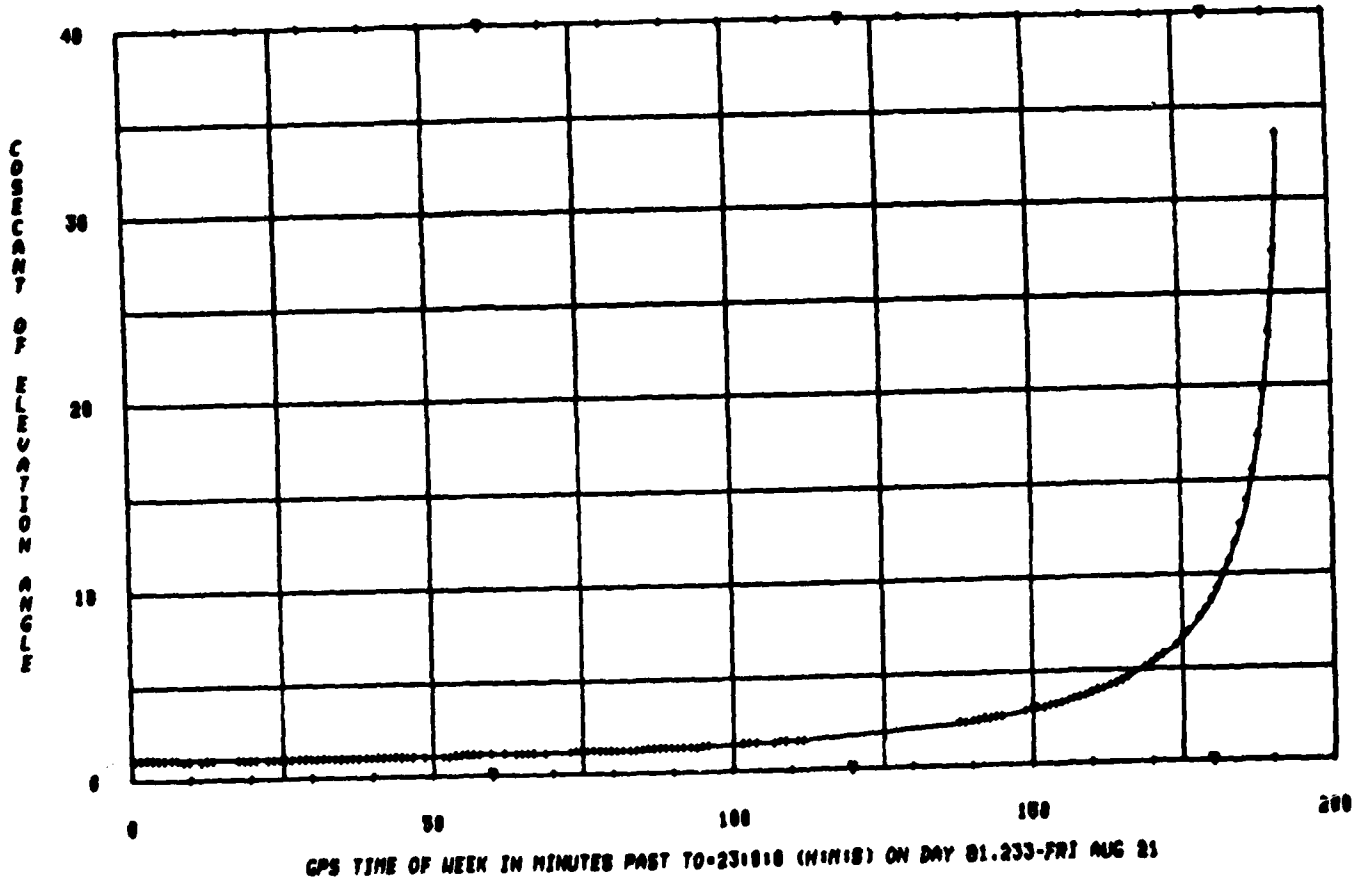

FIGURE 25. COSECANT OF NAVSTAR 3 ELEVATION ANGLE; DAY 81.233.

(NO REFRACTION CORRECTION)

STATISTICS IN MICROSEC

NR-	3	4	5	6
AVE	-81.963	-82.091	-6864.916	-81.:70
SIG	.020	.082	.031	.116
PTS	163	163	163	163
DIFF	.221	.360	.134	.877

DATA PLOTTED FOR CHANNEL 2
AVERAGE SUBTRACTED FOR PLOTTING

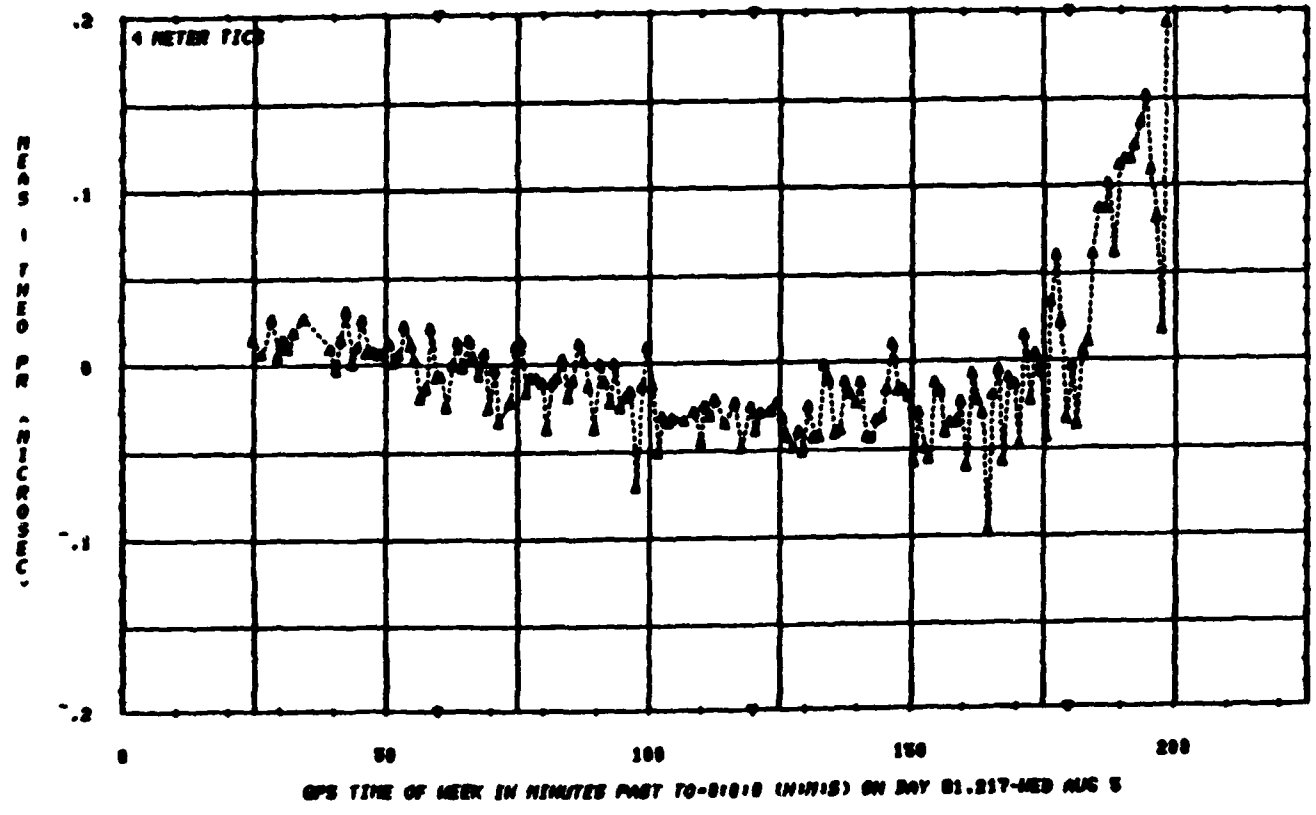

FIGURE 26. L1 C/A-CODE PSEUDORANGE RESIDUALS; X-SET 1; DAY 81.217; NAVSTAR 4.

(NO REFRACTION CORRECTION)

STATISTICS IN NICROSEC

NS-	3	4	5	6
AVE	-81.733	-81.732	-81.686	-81.740
SIG	.861	.868	.848	.828
PTS	173	173	173	173
DIFF	.383	.368	.187	.896

DATA PLOTTED FOR CHANNEL 2
AVERAGE SUBTRACTED FOR PLOTTING

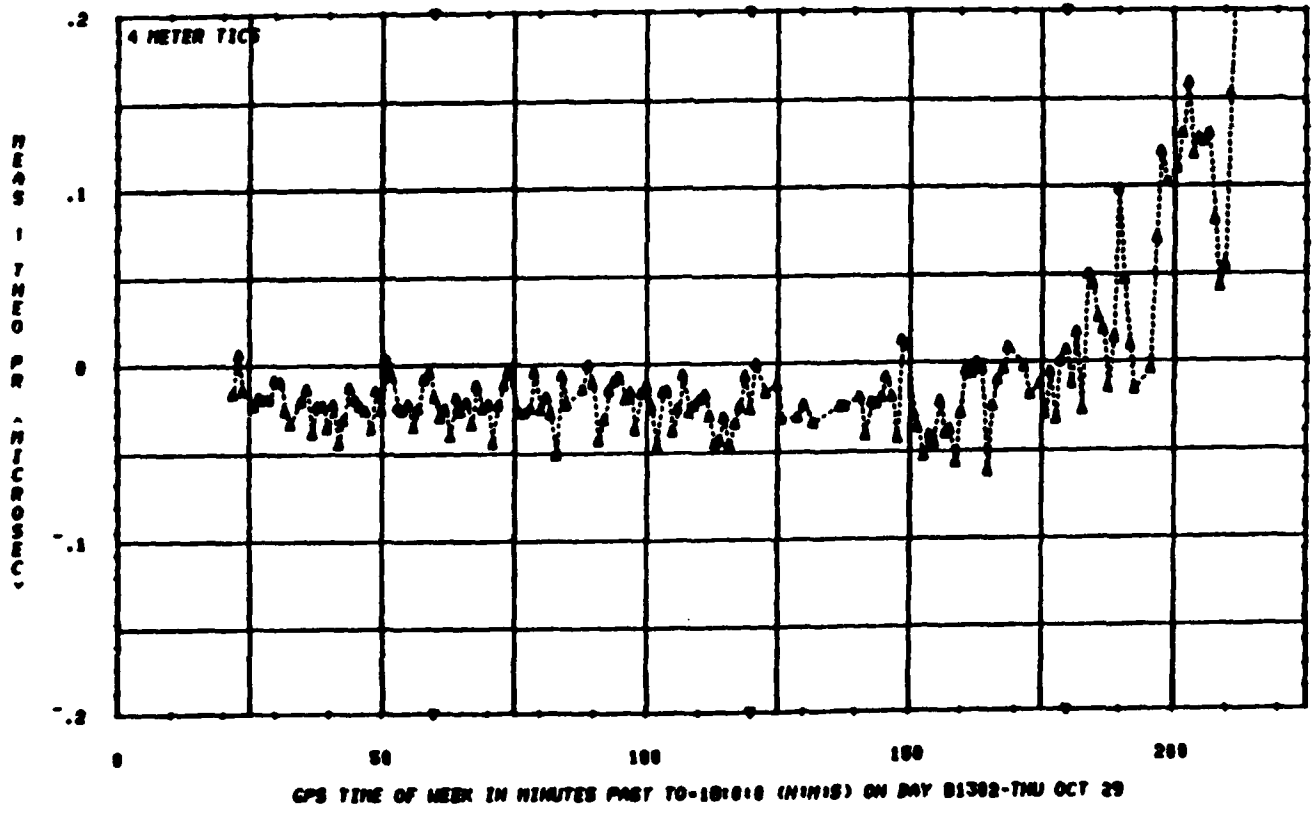

FIGURE 27. L1 C/A-CODE PSEUDORANGE RESIDUALS; X-SET 1; DAY 81.302; NAVSTAR 4.

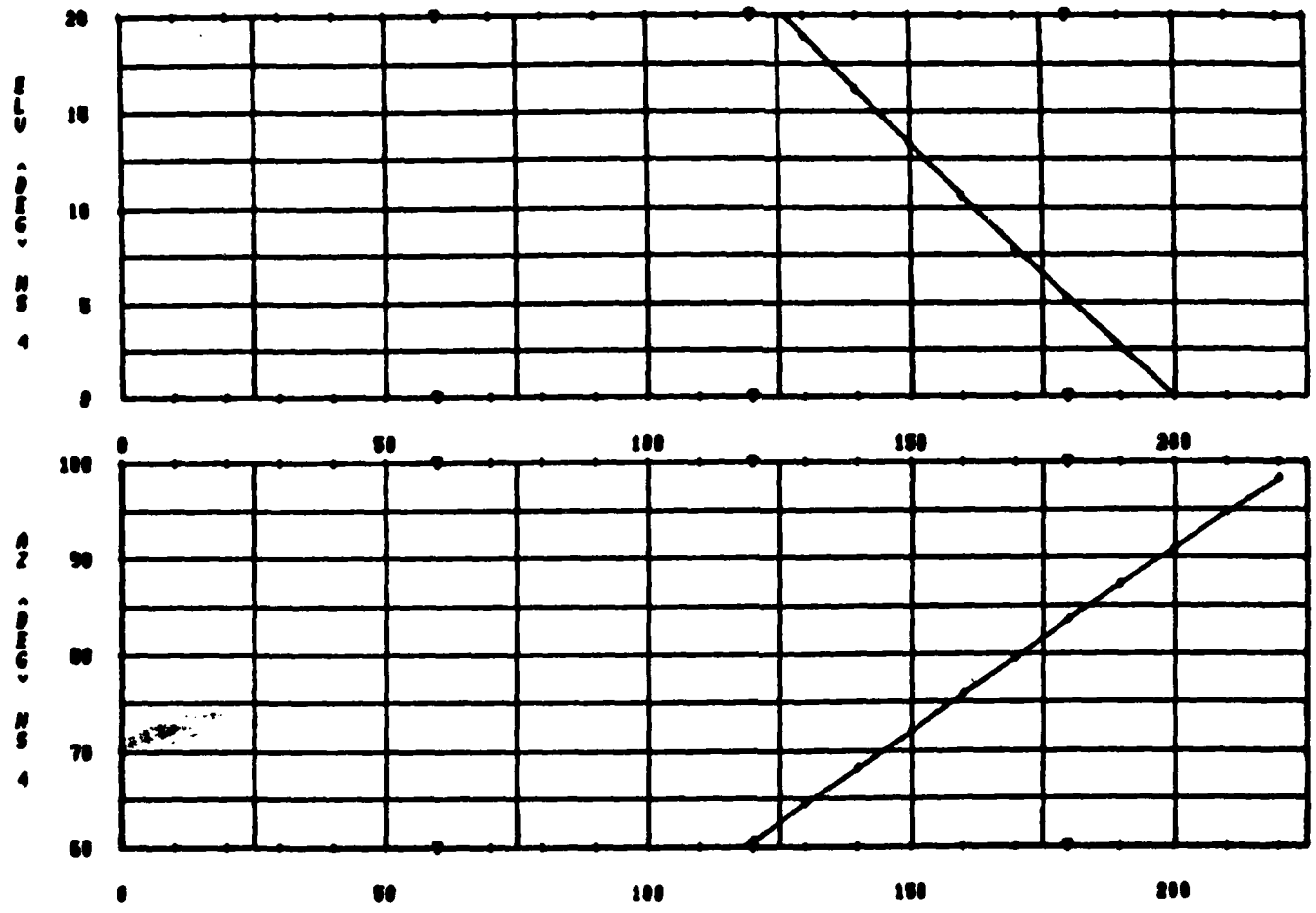

FIGURE 28. ELEVATION AND AZIMUTH ANGLES FOR NAVSTAR 4; DAY 81.217.

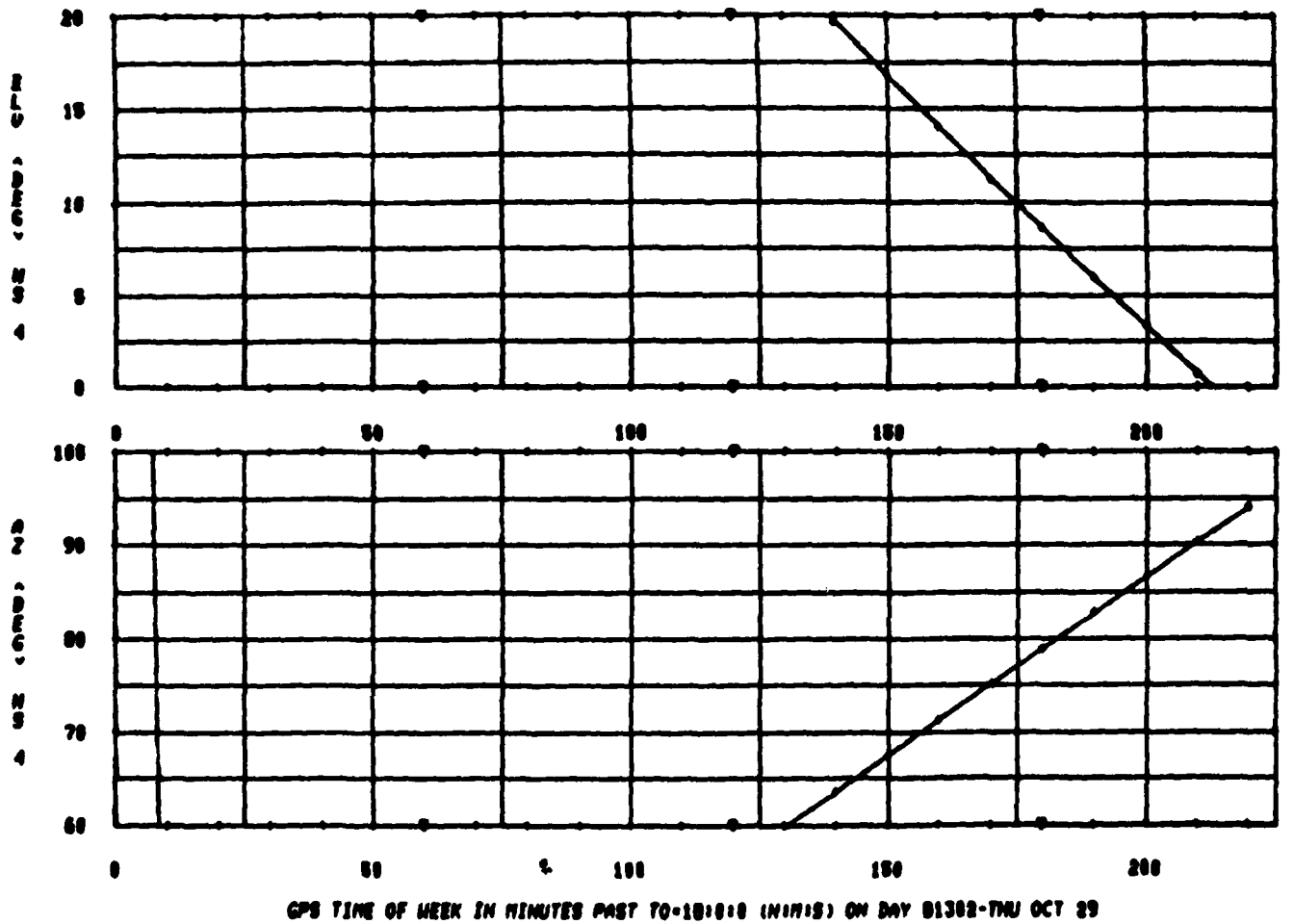

FIGURE 29. ELEVATION AND AZIMUTH ANGLES FOR NAVSTAR 4; DAY 81.302.

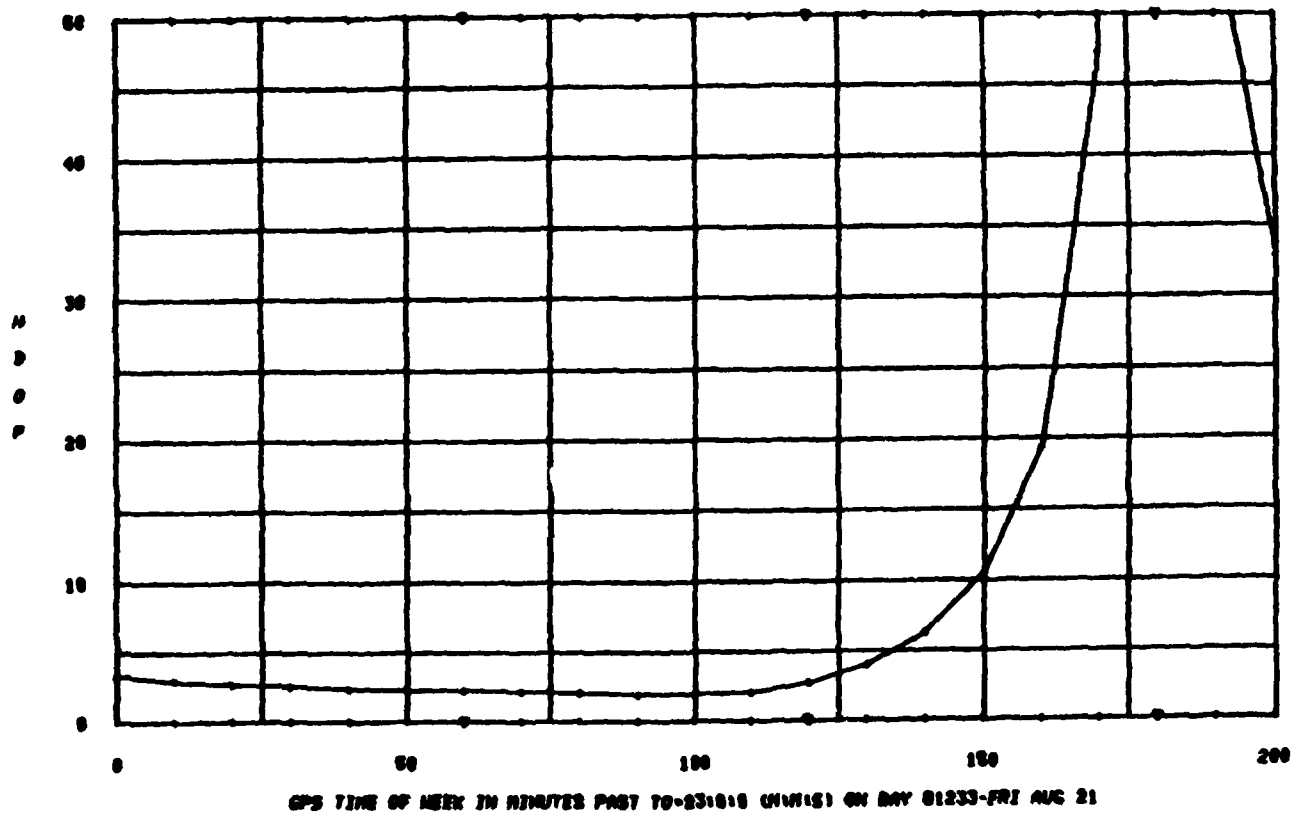

FIGURE 30. HORIZONTAL DILUTION OF PRECISION (HDOP); COMPLETE NAVIGATION SOLUTION; DAY 81.233; NAVSTARS 3, 4, 5, AND 6.

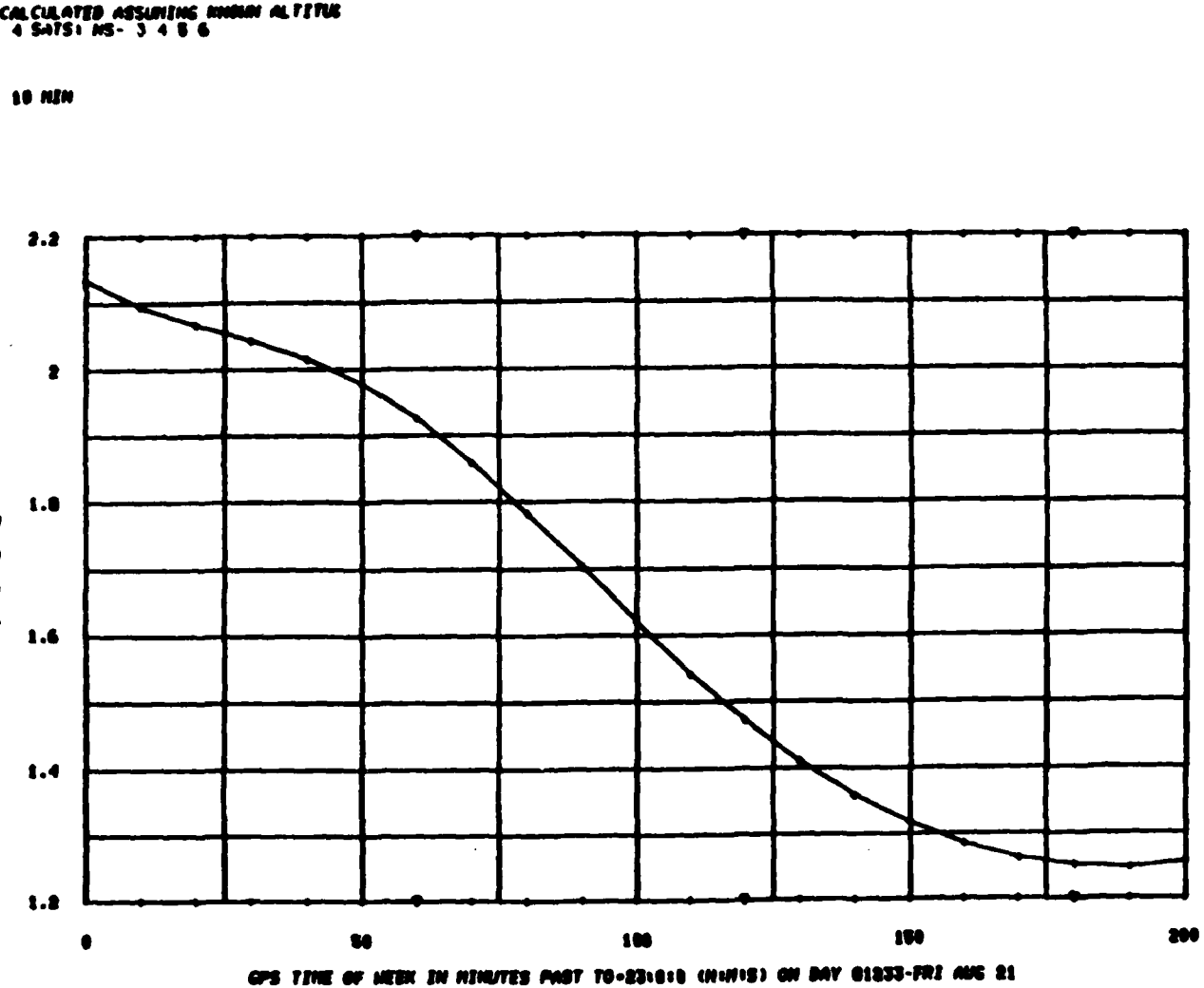

FIGURE 31. HORIZONTAL DILUTION OF PRECISION (HDOP); ASSUMING KNOWN VERTICAL POSITION; DAY 81.233; NAVSTARS 3, 4, 5, AND 6.

APPENDIX B

USCG Tape Log and Processing Summary

Each X-set was assigned to track the L1 signals from the same set of four satellites, NAVSTARs 3, 4, 5, and 6* at a one minute data rate. Before 10/1/81, a TFL cesium standard time base was used; on 10/1/81 and after, a TFL hydrogen maser time base was used.

	Code Assignments			
Date	X-Set 1	X-Set 2		Processed
07/29/81 (81.210)	C/A	P	Yes	
08/05/81 (81.217)	C/A	P	Yes	
08/06/81 (81.218)	-	P	Yes	
08/18/81 (81.230)	P	C/A	Yes	
08/20/81 (81.232)	P	P	Yes,	1st tape with usable iono data
08/21/81 (81.233)	P	P	Yes	
09/01/81 (81.244)	P	C/A	Yes,	bad CH2 on X2
09/02/81 (81.245)	P	C/A	Yes,	bad CH2 on X2
09/15/81 (81.258)	P	Bad Power Supply	Yes,	old ephemeris
10/01/81 (81.274)	P	-	Yes	
10/02/81 (81.275)	P	-	No	
10/13/81 (81.286)	P	-	Yes	
10/22/82 (81.295)	P	-	Yes	
10/23/81 (81.296)	P	-	Yes	
10/27/81 (81.300)	P	-	No	
10/28/81 (81.301)	P	-	Yes	
10/29/81 (81.302)	C/A	-	Yes	
10/30/81 (81.303)	P	-	No	
11/03/81 (81.307)	C/A	-	No	
11/04/81 (81.308)	P	-	No	
11/05/81 (81.309)	C/A	-	No	

*On days 81.218 and 81.232, NAVSTAR 4 was tracked on all channels.

Date	Code Assignments X-Set 1	X-Set 2	Processed
11/19/81 (81.323)	P	-	No
11/20/81 (81.324)	C/A	-	No
11/23/81 (81.327)	C/A	-	No
11/24/81 (81.328)	P	-	No
11/25/81 (81.329)	C/A	-	No
12/3/81 (81.337)	C/A	-	No
12/4/81 (81.338)	P	-	No
12/7/81 (81.341)	P	-	No
12/8/81 (81.342)	C/A	-	No
12/10/81 (81.344)	P	-	No
12/11/81 (81.345)	C/A	-	No
12/16/81 (81.350)	P	-	No

APPENDIX C

As described by Milliken and Zoller (Ref. 1) the GPS navigation solution can be implemented by using vectors and matrix algebra. A least squares solution for the relationship between satellite ranging errors and the user position and clock errors is given by the equation

$$\bar{X}_u = \left| G_u^T G_u \right|^{-1} G_u^T R \qquad \text{(C1)}$$

where

$$X_u = \left| x_u, y_u, z_u, -ct \right|^T , \qquad \text{(C2)}$$

x_u, y_u, z_u, three components of user position,

$-ct$, range equivalent of clock error,

$$G_u = \left| \begin{array}{l} \Gamma_1 \\ \Gamma_2 \\ \Gamma_3 \\ \\ \Gamma_n \end{array} \right| \qquad \Gamma_i = (e_{i1}, e_{i2}, e_{i3}, 1)$$ unit line of sight vector from receiver to satellite i, with e_{ij} direction cosines, n = number of satellites.

$$R = \left| R_1, R_2, R_3, \ldots, R_n \right|^T ,$$

R_i = estimate of error in range of satellite i.

Under the assumption that the ranging errors are random, uncorrelated, and have the same variance, the covariance matrix of the error, $\bar{X}_u$, in the estimate of $\bar{X}_u$ is $\mathrm{Cov}(\delta \bar{X}_u) = (G_u^T G_u)^{-1}$. The diagonal elements are the variance of the estimated user position in each axis and in clock error:

$$\sigma_{xx}^2, \ \sigma_{yy}^2, \ \sigma_{zz}^2, \ \sigma_{tt}^2.$$

The factors which multiply the range uncertainties to get the position and clock uncertainties are referred to as Geometric Dilution of Precision (GDOP) parameters. These are:

$$PDOP = \sqrt{\sigma_{xx}^2 + \sigma_{yy}^2 + \sigma_{zz}^2}\ , \qquad \text{dilution of precision in position in 3-dimensional space}$$

$$HDOP = \sqrt{\sigma_{xx}^2 + \sigma_{yy}^2}\ , \qquad \text{dilution of precision in position in a plane.}$$

$$VDOP = \sigma_{zz}\ , \qquad \text{dilution of precision in position vertical to the plane of HDOP.}$$

$$TDOP = \sigma_{tt}\ , \qquad \text{dilution of precision in time (clock error).}$$

Each term when multiplied by the 1 σ user-to-satellite range error provides the corresponding 1 σ error in position or time. Large values of GDOP parameters indicate a poor navigation solution due to unfavorable satellite geometry and cause a magnification of the ranging errors. Note that the coordinate system has not been specified. If we choose the X axis to be East, the Y axis North, and the Z axis local vertical, the position errors then become errors in longitude, latitude, and altitude.

In general a user will not have a precise estimate of his location nor of his clock error. To solve for these four unknowns he must have ranging data from four satellites. The navigation solution provides him with an estimate of the four unknowns, but the error of these estimates depends partly on the geometry of the satellites viewed and the user. The behavior of HDOP for a user situated at APL and solving for all four unknowns is shown calculated in 10-minute intervals in Fig. 30.

Let this same user assume that his vertical position error is zero so that there is no need to solve for it in equation (C1). The term z_u is removed from X_u which means that the e_{i3} terms are removed from G_u. In this case, there is no VDOP term and the information in the measurement data is used to estimate three variables instead of four. By still using measurements from four satellites the redundant measurement will act to improve the accuracy of the solution, and the HDOP term is expected to be smaller than when vertical position was part of the estimate.

Figure 31 shows the behavior of HDOP for this case and it can be seen that there is a substantial reduction in the magnitude of HDOP, especially during the last half of the pass. It is clear that if a user can justify assuming a zero vertical position error then he will reduce the geometric amplification of his ranging errors.

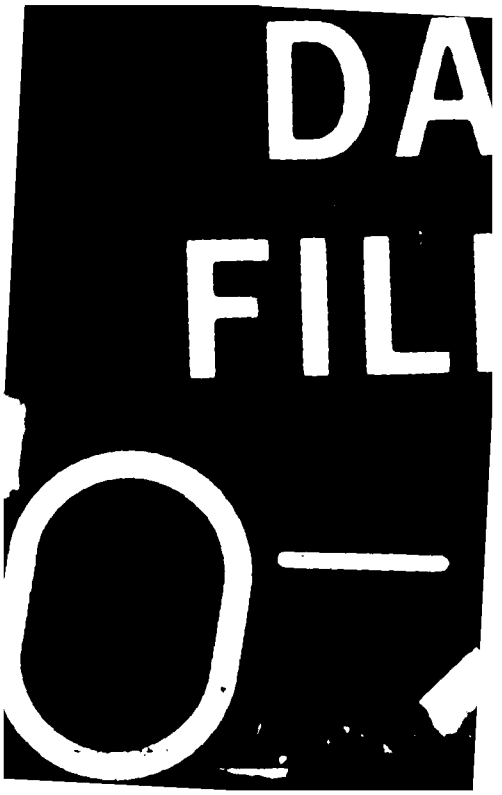
DA
FIL